Effects of simplifying fracture network representation on inert chemical migration in fracture-controlled aquifers

Tristan P. Wellman,[1] Allen M. Shapiro,[2] and Mary C. Hill[3]

Received 25 March 2008; revised 3 October 2008; accepted 29 October 2008; published 22 January 2009.

[1] While it is widely recognized that highly permeable 'large-scale' fractures dominate chemical migration in many fractured aquifers, recent studies suggest that the pervasive 'small-scale' fracturing once considered of less significance can be equally important for characterizing the spatial extent and residence time associated with transport processes. A detailed examination of chemical migration through fracture-controlled aquifers is used to advance this conceptual understanding. The influence of fracture structure is evaluated by quantifying the effects to transport caused by a systematic removal of fractures from three-dimensional discrete fracture models whose attributes are derived from geologic and hydrologic conditions at multiple field sites. Results indicate that the effects to transport caused by network simplification are sensitive to the fracture network characteristics, degree of network simplification, and plume travel distance, but primarily in an indirect sense since correlation to individual attributes is limited. Transport processes can be 'enhanced' or 'restricted' from network simplification meaning that the elimination of fractures may increase or decrease mass migration, mean travel time, dispersion, and tailing of the concentration plume. The results demonstrate why, for instance, chemical migration may not follow the classic advection-dispersion equation where dispersion approximates the effect of the ignored geologic structure as a strictly additive process to the mean flow. The analyses further reveal that the prediction error caused by fracture network simplification is reduced by at least 50% using the median estimate from an ensemble of simplified fracture network models, and that the error from network simplification is at least 70% less than the stochastic variability from multiple realizations.

Citation: Wellman, T. P., A. M. Shapiro, and M. C. Hill (2009), Effects of simplifying fracture network representation on inert chemical migration in fracture-controlled aquifers, *Water Resour. Res.*, *45*, W01416, doi:10.1029/2008WR007025.

1. Introduction

[2] Chemical migration in many fractured aquifers is controlled by the geometry of the fracture network. Late-time tailing in solute breakthrough curves indicates that the structure of a fracture network imposes a multiscaled influence on transport and that dispersion departs from the classic Fickian model [e.g., *Smith and Schwartz*, 1980; *Abelin et al.*, 1987]. Non-Fickan transport is evident in a variety of numerical studies of fractured aquifers [e.g., *Schwartz et al.*, 1983; *Nordqvist et al.*, 1992; *Bear et al.*, 1993], and is observed at the fracture-scale [*Tsang et al.*, 1988; *Mettier et al.*, 2006], field-scale [*Cacas et al.*, 1990a, 1990b; *Becker and Shapiro*, 2000], and kilometer-scale [*Shapiro*, 2001]. Physical explanations of this behavior include the spatial variation of flow velocity within and between fractures [*Becker and Shapiro*, 2000; *Shapiro*, 2001] and a diffusive mass transfer between hydraulically active and quiescent regions of an aquifer [*Cvetkovic et al.*, 1999; *Andersson et al.*, 2004].

[3] Complex patterns of chemical migration can be modeled in a variety of ways, including: discrete fracture network representation (DFN) [*Dershowitz et al.*, 1998], multi-rate mobile-immobile transfer [*Haggerty et al.*, 2001], continuous time random walk [*Berkowitz and Scher*, 1995], stochastic fracture continuum [e.g., *Ando et al.*, 2003], and fractional advection-dispersion [*Benson et al.*, 2000]. In traditional three-dimensional applications, a portion of the aquifer structure is represented explicitly on the model grid using a variety of hard and soft field data, while the effect of the remaining structure is approximated by a stationary equation (e.g., a dispersion function) or under some circumstances is simply ignored. Selecting the proportion of structure that will be represented explicitly is an important decision, one that benefits from a clear understanding of the fractures controlling chemical transport.

[4] It is well recognized that fractures range in size from the pore-scale to the kilometer-scale [e.g., *Bonnet et al.*, 2001]. This presents the possibility that all scales of fractures substantially influence chemical transport through fractured aquifers. Earlier work, however, suggests that "small" fractures or those with poor conductance may be reasonably ignored when networks retain connectivity across

[1]Water Resources Discipline, U.S. Geological Survey, Lakewood, Colorado, USA.
[2]Water Resources Discipline, U.S. Geological Survey, Reston, Virginia, USA.
[3]Water Resources Discipline, U.S. Geological Survey, Boulder, Colorado, USA.

0043-1397/09/2008WR007025$09.00

the region examined [e.g., *Cacas et al.*, 1990a, 1990b; *Hestir and Long*, 1990; *Herbert et al.*, 1991]. Conventional opinion follows that "large" fractures provide the "backbone" of major connected pathways, and "small" fractures may be neglected or coarsely approximated because of their minor contribution to the total volumetric flow [e.g., *National Research Council*, 1996, p. 367]. While this paradigm of "large" fracture dominance may be reasonable under certain circumstances, it is being challenged by recent observations which indicate that "small" pervasive fractures provide important migration pathways at certain spatial and temporal scales [e.g., *Sidle et al.*, 1998; *Kosakowski et al.*, 2000; *Becker and Shapiro*, 2000; *Mettier et al.*, 2006]. The latter is further supported by two-dimensional hierarchical modeling which suggests that small-scale structure may be important in certain cases [*Clemo and Smith*, 1989, 1997]. In all, there are a variety of findings as to which fractures control transport processes, but little certainty as to why or when these differences occur. To understand this relation with greater clarity the influences of the fracture network should be examined using a consistent methodology over a range of conditions where the attributes of the fracture network are known. Analyses should advance beyond the identification of "important" fractures in a generic context since the results may vary depending on the type of transport measure considered, geometry of the fracture network, and degree of network simplification. Even factors unrelated to the network geometry such as plume travel distance may be important considerations.

[5] This investigation evaluates directly the significance of network simplification on chemical migration by systematically eliminating portions of the network structure, and articulates the manner in which transport is altered over a range of fracture network geometries and plume travel distances. A multistep procedure is used to construct a suite of three-dimensional DFN models that honor geologic and hydrologic field observations. The difference in transport predictions between each simplified network model and the corresponding complete network model is considered the error in transport prediction caused by network simplification, which is equivalent to the influence of the removed fractures in controlling transport. The primary goals of this work are: (1) to quantify and characterize the error in transport predictions caused by fracture network simplification for a range of networks, (2) to investigate the correlation between the error in transport predictions and attributes of the fracture network, degree of network simplification, and solute travel distance, and (3) to evaluate methods for reducing the error that is caused by network simplification.

2. Model Development

2.1. Model Specifications

[6] A suite of DFN models is constructed through a multistep process that honors hydrogeologic characteristics observed in crystalline-rock aquifers. The modeled region under consideration is a parallelepiped with dimensions of 60 m x 60 m x 40 m (Figure 1a; "X," "Y," "Z"). Dirichlet hydraulic boundary conditions are applied to the two opposing "Y"–"Z" peripheral faces of the model region such that a 0.05 hydraulic gradient is established collinear to the "X" coordinate axis. A hydraulic gradient of this magnitude falls between precipitous mountain watersheds with regional values of ~0.10 [e.g., *Wellman and Poeter*, 2006] and those of flat lying topography, but the choice of gradient is considered arbitrary since dispersion scales to the flow velocity and no particular field site is considered. Along the four lateral model faces hydraulic head is linearly interpolated as a function of the "X" coordinate axis. Linearly varying hydraulic conditions are preferred since they allow fluid to enter or exit the model periphery from any direction during a simulation and do not artificially alter particle flow paths to the extent that occurs from no-flow conditions.

[7] The DFN generator FracMan is used to construct stochastic fracture networks according to user-specified fracture attributes [*Dershowitz et al.*, 1998]. The generated networks consist of two-dimensional (planar) fractures interconnected in three-dimensional space. Programs associated with FracMan enable the: (1) construction of a finite element mesh patterned after each fracture network, (2) flow simulation via the Galerkin method, and (3) particle tracking using 5000 particles to predict transport [*Miller et al.*, 1999]. The networks are meshed such that each fracture is typically represented by $\sim 10^1 - 10^2$ finite elements. All meshes are examined for quality and modified for proper element aspect ratios.

[8] Fluid movement through the fracture network is simulated at steady state and the resulting flow velocities are used for simulating transport via particle tracking. A contaminant source injection region is centered 10 m from the up gradient model boundary with dimensions 10 m x 10 m x 10 m (Figure 1a; cube). Injected solute particles are distributed among the fractures intersecting the source region according to a flux-based weighting scheme. Particles propagate in a Lagrangian manner through the fracture network by fluid advection, which is a function of the fracture transmissivity and fracture network connectivity, and by intrafracture dispersivity (D) specified by the user. Particle advection is calculated from the magnitude (V) and direction of the flow velocity vector at a specified location. The basic dispersive movement (L) is approximated by the traditional relation

$$L_{dir} = R_N \cdot (2D_{dir}Vt)^{0.5} \quad (1)$$

where the subscript "dir" indicates either a longitudinal or transverse direction relative to the fluid velocity vector, and R_N is a dimensionless random number selected from a standard normal distribution [*Miller et al.*, 1999]. The total particle movement is therefore a combined function of particle advection (Vt) and longitudinal dispersive movement collinear to the flow vector, and a dispersive movement traverse to the flow vector. The extent to which the dispersive gradients are corrected in the code algorithm is undocumented [e.g., *Delay et al.*, 2005]. The significance of this effect is presumed dependant on the geometry of the fracture network, conductance variability between intersecting fractures, and the characteristics of the finite element mesh representing the network. Additional details on flow and transport calculations are provided by *Miller et al.* [1999].

[9] A quality control analysis conducted during this investigation finds that particles may exit the fracture network prior to reaching a model domain boundary. Efforts for minimizing this effect were successful in reducing premature

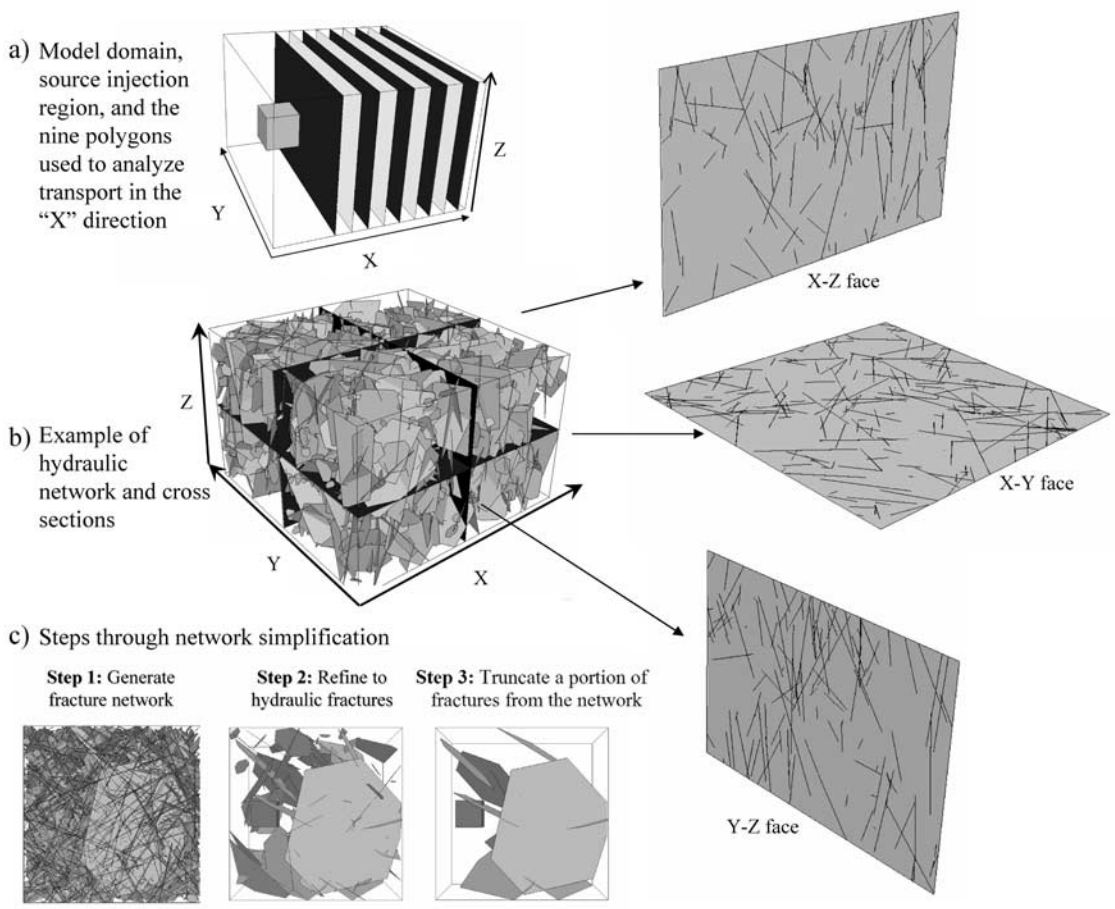

Figure 1. Illustrations show (a) model domain, solute injection region, and nine observation polygons used to examine transport in the 'X' direction, the six observation polygons for analyzing the "Y" direction are perpendicular to those for "X" but are not shown, (b) a refined network of hydraulic fractures with, on average, one hydraulically substantial fracture per randomly located vertical well with a transmissivity $\geq 1 \times 10^{-6}$ m^2 s^{-1}, and (c) a simple example of the steps in simplifying the fracture network structure.

exits to 0–5% of the particle population by adjusting properties of the finite element mesh. Particles exhibiting this trait following the correction procedure are not considered in the transport calculations. Quality control analyses further reveal that if a particle has limited movement for a number of time steps it may be designated immobile within the network. In truth, however, all particles should remain moving at finite velocities during inert transport, even those traveling through relatively immobile flow pathways. These issues provide constraint in the analyses that are appropriate for this investigation. In this work, the migration of mobile particles passing through the fracture network is evaluated.

[10] In addition to transport processes within the fracture network, the interaction between the fracture network and the surrounding rock "matrix" can be important depending on the geologic structure, chemical attributes of the fluid, and time scale of consideration. In this investigation, we focus on the advection and dispersion of inert chemical transport through the fracture network. Molecular diffusion, matrix processes, and fracture-matrix interaction are not considered. The fracture networks evaluated in this work incorporate many of the smaller and less conductive fractures that are typically defined as "matrix" in large-scale models, but do not include all network structure. Notable simplifications to the networks are a prescribed minimum fracture transmissivity of 1×10^{-10} m s^{-2} and a minimum fracture "radius" of 0.3 m, as defined in the next section.

2.2. Fixed Fracture Attributes

[11] The fracture network attributes evaluated in this investigation are derived from a preliminary analysis to assess the computational limits and runtimes of fracture network models using a range of domain sizes and fracture network properties (Table 1). Fracture spacing is assumed to follow an enhanced Baecher model, which is supported by several field observations [e.g., *Priest and Hudson*, 1976; *Baecher et al.*, 1977; *Wallis and King*, 1980; *Dershowitz et al.*, 1998; *Outters and Shuttle*, 2000; *Caine and Tomusiak*, 2003; *Cvetkovic et al.*, 2004]. Fracture networks with clustered fracture centers that are fractal or multifractal also are recognized, but are not considered in this investigation. Each fracture is modeled as an isotropic 6-sided polygon with a corresponding "radius" that is determined by converting polygon area into the form of a circle. For practicality, three orientation sets are defined from a common pattern found at several field sites [*Rouleau and Gale*, 1985; *Burton et al.*, 2000; *Bossong et al.*, 2003; *Watanabe et al.*, 1982; *Hatsuyama et al.*, 1993; *Japan Nuclear Cycle Development Institute*,

Table 1. Fracture Network Specifications

Variable/Parameter	Value/Type
Domain (m)	60 × 60 × 40
Injection Region (m)	10 × 10 × 10
Fracture Sets (3 sets)	A(45%), B(45%), C(10%)
Fracture Orientation	A(315°), B(45°), C(360°)
Fracture Dip	A(90°), B(90°), C(0°)
Orient./Dip Dispersion	Fisher measure = 10.0
Fracture Geometry	6-sided polygon
Min. Fracture Radius (m)	0.3
Max. Fracture Radius (m)	6.0, 12.0, 24.0
Power Length Exponent	1.7, 2, 2.25, 2.80
Spacing Model	Enhanced Baecher
Total P_{32} Density (m^{-1})	1.0, 2.5, 5.0
Aperture (m)	Min:10^{-7}, Max.10^{-3}
Transmissivity (m^2 s^{-1})	Min:10^{-10}, Max.10^{-4}
Fracture Dispersivity (m)	2

1999]. Two orthogonal and steeply dipping fracture sets comprise 90% of the features with mean orientations that dip 90° and trend ±45° to the hydraulic gradient. The remaining 10% of the fractures are represented as subhorizontal with a random trend. A Fisher dispersion of 10.0 introduces random variability in fracture orientation [*Fisher et al.*, 1987; *Dershowitz et al.*, 1999; *Japan Nuclear Cycle Development Institute*, 2000]. Within each fracture the dispersivity of transport paths is set to 2 m. Studies suggest that dispersivity mainly varies as 20% of the fracture radius, with some values ranging between 1 and 200% of the fracture radius [*Neretnieks*, 1980; *Gelhar et al.*, 1992]. Using 20% of the fracture radius, dispersivity is less than 2 m for nearly all fractures considered in this analysis. The effects of dispersivity between 0.5 and 2 m have limited influence on field-scale transport as compared to the macrodispersive effects imposed by the fracture transmissivity distribution and network geometry [*Sawada et al.*, 1999]. There are similar findings in related studies [e.g., *Painter and Cvetkovic*, 2001; *Painter*, 2006].

2.3. Variable Fracture Attributes

[12] The variable fracture attributes in this analysis are the fracture length distribution described in terms of fracture radius, fracture density, and maximum fracture radius. The fracture radius distribution is assumed to follow a power law relation. Key arguments in favor of a power law distribution are the lack of a characteristic length scale in the fracture growth process, and its frequent occurrence in field analyses [*Bonnet et al.*, 2001]. The power length exponent relates fracture size to the frequency of occurrence, and typically ranges from 1.0 to 3.0 for trace length data [e.g., *Adler and Thovert*, 1999; *Bonnet et al.*, 2001, and references therein]. While the precise conversion in power exponent when transitioning from two- to three- dimensional networks is unclear, especially for complex networks or those with multiple sets of fractures, some adjustment is warranted [*Piggot*, 1997; *Bonnet et al.*, 2001; *Darcel et al.*, 2003b]. For this investigation, the power exponents are varied between 1.7, 2.25, and 2.8 as measured by fracture radius (1/2 fracture length), which is the unit used for model input. Power distributions with large exponents have, on average, a greater number of small fractures, and vice versa, which can affect the macroscopic network connectivity [e.g., *Darcel et al.*, 2003a, 2003b]. The second varied parameter is the fracture surface density (P_{32}), which is the total fracture surface area normalized to the sampling volume [*Dershowitz*, 1985]. Reported P_{32} values in crystalline systems often range from 1 to 30 m^{-1}, depending on the location and minimum fracture size considered, with many nonfaulted regions having densities below approximately 5 m^{-1} [e.g., *Niemi et al.*, 2000; *Caine and Tomusiak*, 2003; *Andersson et al.*, 2005]. Here, moderately dense networks with P_{32} densities of 1, 2.5, and 5.0 m^{-1} are selected. Last, the maximum fracture radius is considered, which may affect connectivity across a network [e.g., *Hestir and Long*, 1990; *de Dreuzy et al.*, 2001]. The maximum fracture radii are varied between 6 m, 12 m, and 24 m, which in terms of fracture length (2 · radius) correspond to 20, 40, and 80%, respectively, of the largest model domain dimension (60 m). The maximum fracture radius is used to reflect the influence of a finite model domain where the largest features in the network may be absent or partially clipped by the region of investigation. By varying these three parameters independently there arise 27 (3^3) unique parameter sets to evaluate. In addition, each set is used to construct 10 stochastic fracture models to add a component of network variability. The resulting 270 base fracture networks vary considerably in geometry and complexity. The most complex networks possess in excess of 350,000 fractures in the 60 m x 60 m x 40 m model region with millions of fracture intersections, but overall the range is substantial with some networks possessing relatively few structural features (Figure 2a; 'Total').

2.4. Estimating Fracture Transmissivity

[13] Transmissivity is prescribed for each fracture when using DFN representation. Recently reported and reexamined packer data indicate that fracture transmissivity distributions may exhibit tailing and irregularity that is inconsistent with traditional models [e.g., *Niemi et al.*, 2000; *Gustafson and Fransson*, 2005; *Shapiro et al.*, 2007]. A simple radius-based approach with stochastic variability is developed to estimate fracture transmissivity. A relation is first used to correlate fracture radius (f_r) to fracture aperture (A) by the power law relation

$$f_r = \alpha A^{\eta}, \tag{2}$$

where α and η are the proportionality and scaling coefficients with units of [$m^{1-\eta}$] and [−], respectively, with η ranging between 0.5 and 2.0 [*Walsh and Watterson*, 1988; *Scholz and Cowie*, 1990; *Vermilye and Scholz*, 1995; *Hatton et al.*, 1994; *Johnston and McCaffrey*, 1996; *Walmann et al.*, 1996; *Renshaw and Park*, 1997]. Strongest support of this relation suggests that the correlation coefficient between fracture radius and fracture aperture may be as high as 0.90 [*Chiles and de Marsily*, 1993], but for many sites the relation will be nonlinear in log space over large scale ranges and will likely possess substantial scatter [*Renshaw and Park*, 1997; *Olson*, 2003]. For the 60 m scale evaluated in this work a log linear approximation is assumed. Combining equation (2) with the conductance term from the 'cubic law' yields a relation between the fracture transmissivity (T) and fracture radius that is given in the form

$$Log_{10}T = Log_{10}\left(\beta f_r^{3/\eta}\right) + \varepsilon, \tag{3}$$

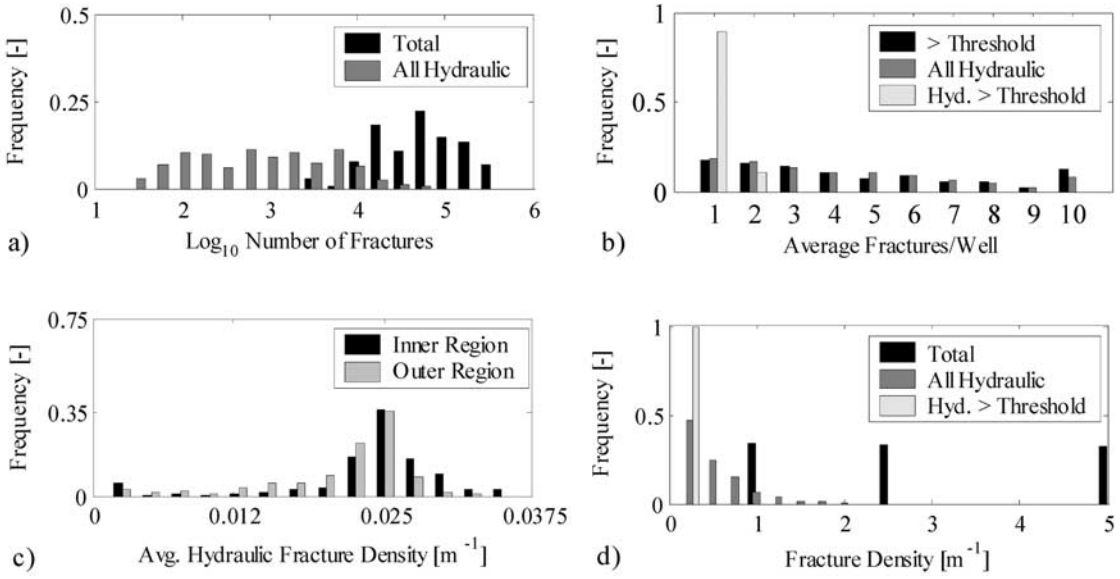

Figure 2. Distributions of the total and hydraulic fractures: (a) total bulk fractures versus total hydraulic fractures, (b) average fractures per well, (c) hydraulic fracture densities (inner and outer refinement regions as described in the text), and (d) P_{32} fracture densities. "Total" $\equiv$ total fractures, " >Threshold" $\equiv$ all fractures with a transmissivity $\geq 1 \times 10^{-6}$ m^2 s^{-1}, "All hydraulic" $\equiv$ all hydraulic fractures, and "Hyd. > threshold" $\equiv$ hydraulic fractures with a transmissivity $\geq 1 \times 10^{-6}$ m^2 s^{-1}.

where β is an effective coefficient with units [$m^{(2\eta-3)/\eta}$ s^{-1}], and ε is a random $\log_{10}$ variability term with units [$\log_{10}$(m^2 s^{-1})]. A random term (ε) jointly approximates the variability in the relations between the fracture radius and physical aperture, and between fracture radius and transmissivity.

[14] Results from several field analyses are used to estimate the parameters in equation (3). Research at the Romuvarra site [e.g., *Niemi et al.*, 2000], USGS Mirror Lake site [e.g., *Shapiro*, 2001; *Shapiro et al.*, 2007], Äspö Hard Rock Laboratory [e.g., *Winberg*, 1996], and the *Japan Nuclear Cycle Development Institute* [1999] collectively suggest that $\log_{10}$ transmissivity values generally vary between -5 to -12 [$\log_{10}$(m^2 s^{-1})] for fractures ranging from one to several meters in radius. Additional work at the Äspö Laboratory reports decameter-scale water-bearing fractures occurring along drifts with $\log_{10}$ transmissivity values ranging from -4 to -6 [$\log_{10}$(m^2 s^{-1})], and values below -6 [$\log_{10}$(m^2 s^{-1})] for the smaller meter-scale fractures [*Mazurek et al.*, 2003]. This suggests a partial overlap in the ranges of transmissivity at the meter- and decameter- scales. Herein, it is hypothesized that a similar overlap exists at other fracture scales (radii), dependent on the parameters in equation (3) and the scales evaluated. It is further assumed that fracture transmissivity at the microscale is, on average, lower than fracture transmissivity at much larger scales. The latter assumption is supported from studies where major conductive faults possess transmissivity values several orders of magnitude greater than the surrounding background fractures [e.g., *Tiren*, 1989; *Black et al.*, 1990; *Olsson*, 1992; *Barton et al.*, 1995; *National Research Council*, 1996; *Seaton and Burbey*, 2005; *Gräsle et al.*, 2006]. However, a perfect scale relation does not exist since faults may possess relatively low transmissivity and act as flow barriers depending on their structural characteristics [e.g., *Caine et al.*, 1996]. Moreover, even small changes in individual fault zone "components" can lead to permeability variability of up to 5 orders of magnitude [*Caine and Forster*, 1999].

[15] The above findings suggest a moderate increase in transmissivity from the microscales to macroscales with a substantial range of transmissivity values at individual length scales. To approximate the behavior for the aforementioned sites collectively, we set (η) and (β) in equation (3) to 1.875 and 3×10^{-9} [$m^{(2\eta-3)/\eta}$ s^{-1}], respectively, and for simplicity define ε using a uniform random variable spanning five orders of magnitude (± 2.5 deviating from $\beta l^{3/\eta}$ in log space). Other suitable functions of ε are plausible in the event that additional information is available. Figure 3 provides an example of the resulting transmissivity distribution using a fracture network with a power length distribution exponent of 1.7 and maximum fracture radius of 24 m.

[16] A final point of consideration is that the physical aperture (A, equation (2)) and transport aperture (A_{trans}) are different measures distinguished by the effects of fracture surface roughness and the geometry of contact surfaces along the fracture plane [e.g., *Pyrak-Nolte et al.*, 1987; *Tsang et al.*, 1988; *Tsang and Tsang*, 1989]. For modeling transport, a transport aperture is employed, which controls the solute velocity along the fracture plane. A coarse approximation is used to relate transmissivity to transport aperture through the empirical relation

$$A_{trans} = T^{0.5} \cdot D, \tag{4}$$

where D is a coefficient set to 0.5 [s$^{1/2}$] [e.g., *Dershowitz et al.*, 1999; *Outters and Shuttle*, 2000; T. Doe, unpublished report, 1993]. This relation is used in lieu of the cubic law because of its purported superior fit to transport processes under field conditions. The above methods are used for the

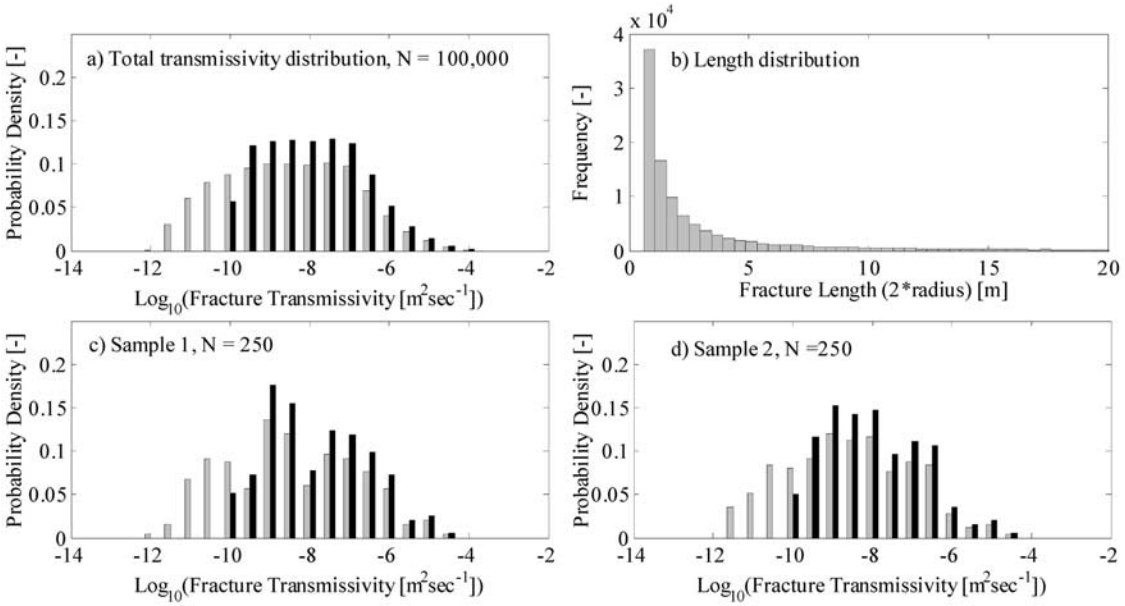

Figure 3. Example of the fracture transmissivity characteristics in a network with a power length exponent of 1.7 and maximum fracture radius of 24 m: (a) 'true' histogram, (b) fracture radius distribution, and (c) and (d) sample histograms using 250 randomly selected observations. For Figures 3a, 3c, and 3d, gray bars reveal all values, and black bars show values greater than a field detection limit of 1×10^{-10} m^2 s^{-1}.

estimation of transmissivity and transport aperture for all fractures considered in this investigation.

2.5. Network Refinement and Simplification

[17] The resulting suite of fracture network models is further conditioned to the hydraulic characteristics observed in fractured crystalline aquifers. The conditioning requires both a methodology for refining fracture networks and an assessment of the hydraulic characteristics observed in fractured crystalline aquifers, as discussed below. The conditioned fracture network models are then simplified using a systematic procedure, thereby creating additional models with varying degrees of network simplification. The resulting suite of conditioned models with varying degrees of simplification is used to evaluate the effects of network simplification on chemical transport.

2.5.1. Field Observations of Hydraulic Characteristics in Fractured Aquifers

[18] It is established from the examination of well-bores that the density of hydraulically substantial fractures in crystalline aquifers is low in relation to the total fracture density [e.g., *Snow*, 1968; *Shapiro and Hsieh*, 1991, 1994; *Poeter et al.*, 2003]. Detailed subsurface investigations at the Stripa Site, Sweden, reveals that a single fracture may contribute ~80% of the water production along a 10 m x 50 m cross-section [*Olsson*, 1992]. The pattern of few hydraulically substantial fractures is also present along drifts at the Äspö Laboratory where more than 100 free-flowing, steeply dipping, decameter-scale fractures are observed with spacing of ~10–20 m with individual transmissivity values above 10^{-6} m^2 s^{-1}, rendering a hydraulic fracture density of 0.05–0.10 fractures m^{-1} [*Mazurek et al.*, 2003]. Moreover, at the U.S. Geological Survey (USGS) Mirror Lake Research Site, USA, results show that between depths of 20 and 80 m only one to three hydraulically substantial fractures produce more than 90% of the water, suggesting that the hydraulic fracture density is between 0.02 and 0.05 fractures m^{-1} for fracture clusters with transmissivity values above 10^{-5} m^2 s^{-1} [*Paillet*, 1993; *National Research Council*, 1996]. More recent analysis at Mirror Lake, however, suggests that hydraulic fracture density is often toward the lower end of this range [*Johnson*, 1999]. In Turkey Creek Basin, USA, data from 1,117 drillers' logs reveal that the average hydraulic fracture density is between 0.025 and 0.040 fractures m^{-1} [*Poeter et al.*, 2003]. The largest values occur mainly in the highly fractured (weathered) zone in the upper 30 m from the land surface, below which there is a fairly constant hydraulic fracture density of 0.025 fractures m^{-1} using 30 m bin intervals to depths of 200 m. In turning to the Kamaishi mine, Japan, the hydraulic fracture density is notably greater where major water-bearing fractures along horizontal drifts occur between ~0.1 and 0.2 fractures m^{-1} [*Japan Nuclear Cycle Development Institute*, 1999]. In considering the aforementioned studies collectively, the average density of hydraulically substantial fractures for a group of wells is estimated between ~10^{-2} and 10^{-1} fractures m^{-1}, depending on the field site and the metric used to distinguish hydraulically substantial fractures. Some of these findings may reflect measurement bias, as when evaluating near vertical fractures using vertical well-bores that can lead to artificially low observed frequencies. For this study, the hydraulically substantial fractures are identified as those with transmissivity values above 1×10^{-6} m^2 s^{-1}. The assumed average hydraulic fracture density is 0.025 fractures m^{-1} within a representative group of vertical well-bores.

2.5.2. Conditioning Fracture Networks

[19] The term 'refinement' is used to indicate the process of selecting hydraulic fractures from the bulk fracture network. During refinement there is a separate iterative

adjustment in the amount of fractures intersecting the model boundary and remaining internal fractures. For each iteration there is an examination of the average number of hydraulically substantial fractures intersecting 200 randomly selected vertical well-bores penetrating the fracture network. For the condition selected there should be one hydraulically substantial fracture per well, on average, with a transmissivity greater than or equal to 1×10^{-6} m^2 s^{-1} that has a sufficient fluid source. For a fracture to possess a sufficient fluid source, it is assumed there is at least one network pathway from the fracture to a model domain boundary. To meet or exceed the prescribed minimum fracture transmissivity of 1×10^{-6} m^2 s^{-1} at a well, there must be at least one pathway where all of the fractures have a transmissivity equal to or greater than 1×10^{-6} m^2 s^{-1}. A three-dimensional percolation analysis is used to examine the fracture network pathways between the fractures intersecting each well and the model boundaries. Fracture transmissivity is examined concomitantly to determine whether the conductance criterion is met.

2.5.3. Analysis of Network Conditioning

[20] The refinement procedure yields hydraulic fracture networks with 10^1–10^5 fractures within the selected 60 m x 60 m x 40 m model region (Figure 2a). Figure 1b shows an example of a refined hydraulic network with an intermediate number of fractures ($\sim 10^3$) relative to the range of hydraulic networks produced. Collectively, results indicate that the refinement procedure achieves the prescribed target of one hydraulically substantial fracture per well (Figure 2b). The total hydraulic fractures in a network is typically much greater than the number of hydraulically substantial fractures because: (1) most fractures have transmissivity values below 1×10^{-6} m^2 s^{-1} but still form transport pathways, and (2) the pathways consisting of mainly high−conductance features may be ''bottlenecked'' by as little as one low-conductance feature, thereby reducing flow to the entire pathway and removing it from consideration as a sufficient fluid source. The analysis of hydraulically substantial fractures is used to select the proportion of total fractures that is needed to match well observations, but all hydraulically connected features remain part of the hydraulic network.

[21] To further evaluate the refinement method, the 60 m × 60 m × 40 m model domain is separated into two parts; an inner subregion with dimensions of 30 m × 30 × 20 m centered in the middle of the model domain, and an outer subregion consisting of the remaining volume of the model domain. Each subregion is examined separately to determine if edge effects are present. The results show that the hydraulic densities in the inner and outer subregions are both near the selected hydraulic fracture density of 0.025 fractures m^{-1}, indicating that on average no edge effects exist [*Moreno and Neretnieks*, 1993] (Figure 2c). Figure 2d gives the distribution of fracture density, which indicates a heavy tail when evaluating all networks collectively. In short, the refinement procedure honors the selected hydraulic density, and is used to convert the 270 bulk fracture networks into 270 networks of hydraulically active fractures.

2.5.4. Simplification of Network Structure

[22] The above steps detail how the suite of hydraulic fracture networks is generated and parameterized. The primary goal of this investigation is to evaluate the effects of simplifying the fracture network structure on inert chemical transport. Network simplification is performed by removing fractures from each of the 270 hydraulic fracture networks that fall below specified thresholds (levels) (Figure 1c). Fractures are removed iteratively below specified fracture radii (0.375, 0.75, 1.5, 3.0, 6.0 m) and fracture transmissivity (1×10^{-9}, 1×10^{-8}, 1×10^{-7}, 1×10^{-6}, 1×10^{-5} m^2 s^{-1}). The specified thresholds are increased from small to large until either the last network simplification level is achieved or percolation (i.e., network connectivity) is severed, in which case the model is not used. A model is considered connected if there is at least one hydraulic connection between the particle source region and a model boundary (Figure 1a). Including the 270 original hydraulic fracture networks the systematic simplification of the fracture network structure creates a total of 2780 DFN models that are evaluated in this analysis.

3. Evaluation of Transport

[23] Transport behavior is examined from the temporal moments of particle breakthrough at 15 locations. Breakthrough curves are commonly described adequately by orders up to four or five, although higher orders may be required for multipeaked or very complex breakthrough [*Harvey and Gorelick*, 1995; *Luo et al.*, 2008]. Breakthrough curves are examined in the ''X'' coordinate direction (Figure 1; ''X'' coordinate direction) using nine rectangular observation polygons measuring 60 m × 40 m that trend orthogonal to the hydraulic gradient, beginning at 2.5 m downstream from the injection region and then for eight additional locations with 5 m separation. In the ''Y'' coordinate direction breakthrough curves are examined using six polygons, oriented orthogonal to those in the ''X'' coordinate direction, beginning at 2.5 m from each side of the injection region with 5 m spacing thereafter for two additional distances. The mobile particle transport across the 15 observation polygons is examined.

[24] Absolute temporal moments of the breakthrough curves are described as

$$\mu_n^{/}(\mathbf{\Omega}) = \frac{1}{M_{tot}} \int_0^\infty t^n q C(\mathbf{\Omega}, t) dt \approx \frac{1}{N_p} \sum_{i=1}^{N_p} (t_i)^n, \tag{5}$$

where $\mu_n^{/}(\mathbf{\Omega})$ represents the nth absolute temporal moment of the mass-volume ratio of flux-averaged solute concentration ($C(\mathbf{\Omega},t)$) crossing a fixed location ($\mathbf{\Omega}$) at time t with volumetric flux q and total injected solute mass M_{tot}. The fraction $\frac{qC(\mathbf{\Omega},t)}{M_{tot}}$ is the probability density function often denoted $f(t)$. The summation term is an approximation of the integral using particle tracking where t_i is the arrival time of particle i and all particles (N_p) consist of equal mass. The first absolute moment ($\mu_n^{/}(\mathbf{\Omega})$) is the mean arrival time of solute mass and is used for defining the central moments

$$\mu_n(\mathbf{\Omega}) = \frac{1}{M_{tot}} \int_0^\infty \left(t - \mu_1^{/}(\mathbf{\Omega})\right)^n q C(\mathbf{\Omega}, t) dt \approx \frac{1}{N_p} \sum_{i=1}^{N_p} \left(t_i - \mu_1'\right)^n. \tag{6}$$

The second, third, and fourth central moments in equation (6) lead to approximations of the arrival-time variance ($\mu_2(\mathbf{\Omega})$), skewness ($\mu_3(\mathbf{\Omega})/\mu_2^{3/2}(\mathbf{\Omega})$), and kurtosis (($\mu_4(\mathbf{\Omega})/\mu_2^2$

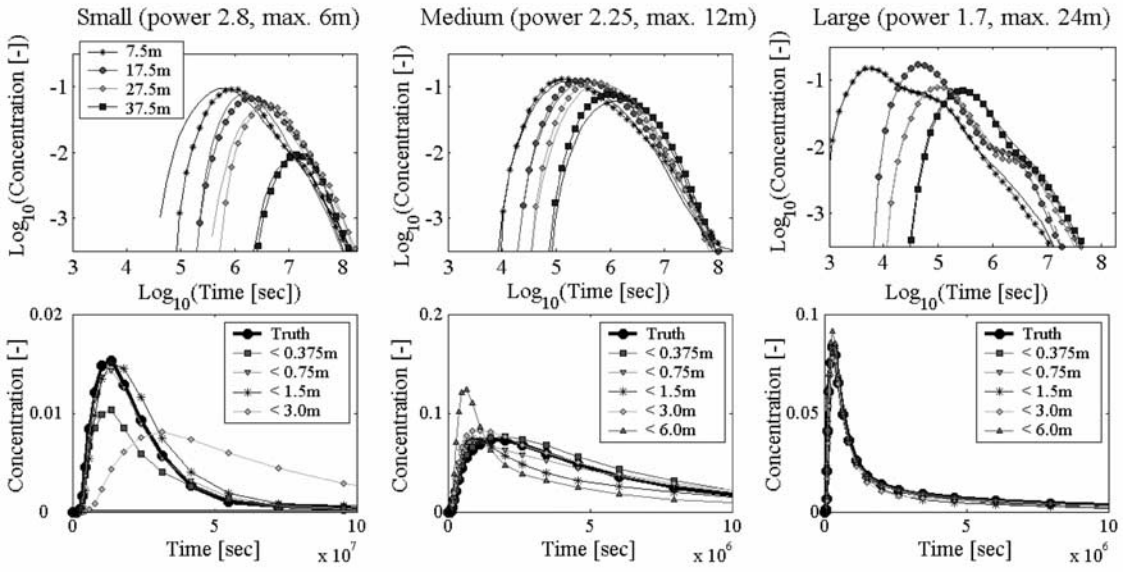

Figure 4. (top) Examples of plume behavior (C/C_0) for small-, medium-, and large- sized fracture populations as noted by the power length exponent and maximum fracture size (columns) in log space. The lines without symbols reveal the effects from removing fractures <1.5 m radius. (bottom) The effect of network simplification below ('<') different fracture radius thresholds in linear space for a single observation distance of 32.5 m for each fracture population. The "<6.0 m" simplification is not included for the small network because network connectivity is severed.

(Ω))−3) of the breakthrough curves, respectively. The variance is a measure of the spread about the mean arrival time. The skewness describes the asymmetry of the breakthrough curve in a temporal sense, where positive values describe breakthrough curves with late-time tailing and negative values describe breakthrough curves with a long early time rise, the former of which is most typical. Kurtosis is a measure of 'peakedness'. Breakthrough curves with a high kurtosis have sharper peaks and fatter tails, whereas low values indicate rounded peaks with broader shoulders. For Gaussian distributions it is noted that skewness and kurtosis are null.

[25] In examining transport, there are both strengths and limitations to using linearly varying boundary conditions along the lateral faces of the model domain. Linearly varying conditions are chosen for their greater realism and smaller influence on transport dynamics as compared to no flow conditions, but since transport particles may exit across the lateral edges of the model only a portion of the particle population may be considered when examining transport. The effects of network simplification are determined in an effective sense at 15 defined polygon locations within the model domain. The number of particles that cross each polygon is the mass arrival at that location.

[26] The five temporal moment measures of particle arrival are determined at each of the 15 observation polygons in each of the 2780 three-dimensional DFN models evaluated in this investigation. Multiple analyses are presented systematically to evaluate the effects of simplifying the fracture network on transport predictions. The analyses are organized as follows: (1) breakthrough curves are first presented to provide a visual description of transport in networks with and without simplification, (2) correlation between moment error caused by simplification and the corresponding 'true' moment values is used to evaluate whether prediction error tends to change with moment magnitude, (3) moment error is evaluated as a function of network simplification to reveal error variability and relative sensitivities, (4) two categories of moment error are identified and examined by the probability that they occur under different aquifer conditions compared to what is statistically expected by random selection, (5) relations between moment error and the network characteristics, travel distance, and degree of network simplification are examined simultaneously using multivariate regression to identify the relative influences of each attribute, (6) the significance of network simplification is evaluated using cumulative error distributions and average errors from select parameter combinations, and lastly (7) error minimization is explored using ensemble averaging.

3.1. Breakthrough Curve Behavior

[27] To illustrate the range of observed transport behavior, three examples are provided with relatively 'small'-, 'medium'-, and 'large'- sized fracture populations, as determined by the power length exponents (2.8, 2.25, 1.7) and maximum fracture radii (6 m, 12 m, 24 m), respectively (Figure 4). All networks have the highest fracture surface density (P_{32}) of 5.0 m^{-1}. In the top row of plots, the breakthrough curves for the complete (i.e., "true") hydraulic network and one simplified hydraulic network (>1.5 m fracture radius) are presented. The corresponding bottom graphs show the effect of simplification by fracture radius at a fixed distance of 32.5 m (i.e., 32.5 m away from the source injection in the "X" direction). In visually examining several plumes we find substantial variation in the breakthrough curve behavior. As a quantitative reference the mass arrival, mean arrival time, and variance of arrival time vary approximately four, four, and nine orders of magnitude,

Table 2. Correlation Coefficients Between Prediction Error and the "True" Moments of Arrival as Measured in Breakthrough Curves[a]

Direction	Truncation	Mass	Mean	Variance	Skewness	Kurtosis
collinear 'xx'	radius	0.08	0.42	0.14	*0.55*	*0.64*
collinear 'xx'	transmissivity	0.12	*0.56*	*0.88*	*0.67*	*0.73*
orthogonal 'yy'	radius	0.18	0.25	−0.03	*0.55*	*0.61*
orthogonal 'yy'	transmissivity	0.19	0.09	0.04	*0.67*	*0.72*
	Average:	0.14	0.33	0.26	*0.61*	*0.68*

[a]High values (italic) indicate errors will often increase with increasing moment measure.

respectively. In some cases breakthrough curve tails are Gaussian-like, as for instance in the 'small' fracture network at 37.5 m from the injection region. However, for the remaining 94% (15/16) of the cases presented there is tailing in the breakthrough curves at later time. In general, concentration peaks may be rounded, flat, or somewhat pointed in their geometry. Curves may exhibit multiple log linear segments that suggest a hierarchical influence, which is especially evident in the 'large' network example where the largest features are present. Early time slopes are often shallower than those at late-time, and are more variable. The most common patterns identified are tailing at later time, hierarchical influences, and an evolution in plume shape with increasing travel distance.

3.2. Correlation of Moment Error to Moment Magnitude

[28] The correlation between moment error caused by network simplification and the corresponding true moments is determined and analyzed (Table 2). The significance of error magnitude is addressed in sections 3.6 and 3.7. Moment error is determined by the residual between the predicted temporal moments using a simplified network and the respective "true" moments predicted from the complete network (i.e., predicted - true). The same convention is used for all of the analyses in this study. Results indicate that the correlation coefficient between the true mass arrival and the error in predicting mass is low (0.14). The correlation coefficients for the "true" mean and variance of particle arrival times is 0.33 and 0.26, respectively, approximately double that for the mass arrival. Correlations for skewness and kurtosis are approximately quadrupled as compared to the mass arrival at 0.61 and 0.68, respectively. The latter findings are most significant and suggest that the prediction of complex plume behavior, such as plume tailing and asymmetry, have higher percentages of error caused by fracture network simplification when considering all results collectively.

3.3. Error Characteristics by Network Simplification

[29] The error in transport prediction is examined as a function of the degree of network simplification by fracture radius (Figures 5a–5e) and fracture transmissivity (Figures 5f–5j) in the "X" coordinate direction. Plots are ordered by row from top to bottom for the particle mass, and the mean, variance, skewness, and kurtosis of particle arrival times, respectively. The left plot axis is the dimensionless moment error calculated by normalizing each error value by the standard deviation of the 'true' moment distribution from the complete hydraulic network. Normalization by the standard deviation allows for a useful comparison of the relative changes in moment error and is mathematically defined in all cases. Absolute error will be addressed in sections 3.6 and 3.7. The black lines and bounding gray regions indicate the median and 25th to 75th percentiles of the normalized errors, respectively. The right axis indicates the frequency (number of cases) that a condition occurs for all models at any of the nine observation locations in the 'X' coordinate direction. The results indicate that frequency decreases with network simplification due to diminishing network connectivity. A reduction in network connectivity occurs because under minor amounts of fracture network simplification there is greater likelihood of maintaining percolation across the model domain as compared to cases with major network simplification.

[30] Using the aforementioned convention, a positive prediction error signifies over prediction of the temporal moment magnitude as a result of fracture network simplification, while a negative error indicates under prediction. At the lowest level of simplification moment error is relatively small. The largest errors occur at the intermediate and largest levels of network simplification. Despite this general trend of increasing error magnitude with added network simplification there are many cases at the largest level of network simplification where the error from network simplification is relatively small and instances at the smaller and moderate levels of network simplification where error is relatively large. This implies that the threshold value used for network simplification is not a strong indicator of prediction error for a specific fracture network structure. Moreover, direct examination of the results shows that the sign of prediction error may reverse when additional structure is removed from the same fracture network, indicating that moment error caused by simplification of a specific network is not invariably of one sign or the other. It is also found that the distribution of error is not Gaussian for the population as a whole, but rather approximates a double exponential (i.e., Laplace) distribution that may be asymmetric. The asymmetry is evident by examining the ranges between each median value and the corresponding 25th and 75th percentiles at each network simplification level. The number of positive or negative errors is approximately equal except in cases where the median error is notably below zero. In using the range of dimensionless error as a metric to estimate parameter sensitivity, we find that the mass arrival is most sensitive to network simplification, followed in decreasing order by the skewness, kurtosis, mean, and variance of particle arrival times.

[31] In all, the findings indicate that: (1) error distributions are not Gaussian for most cases examined, (2) the sign of the prediction error may change by removing different amounts of structure from the same network, (3) structural simplifi-

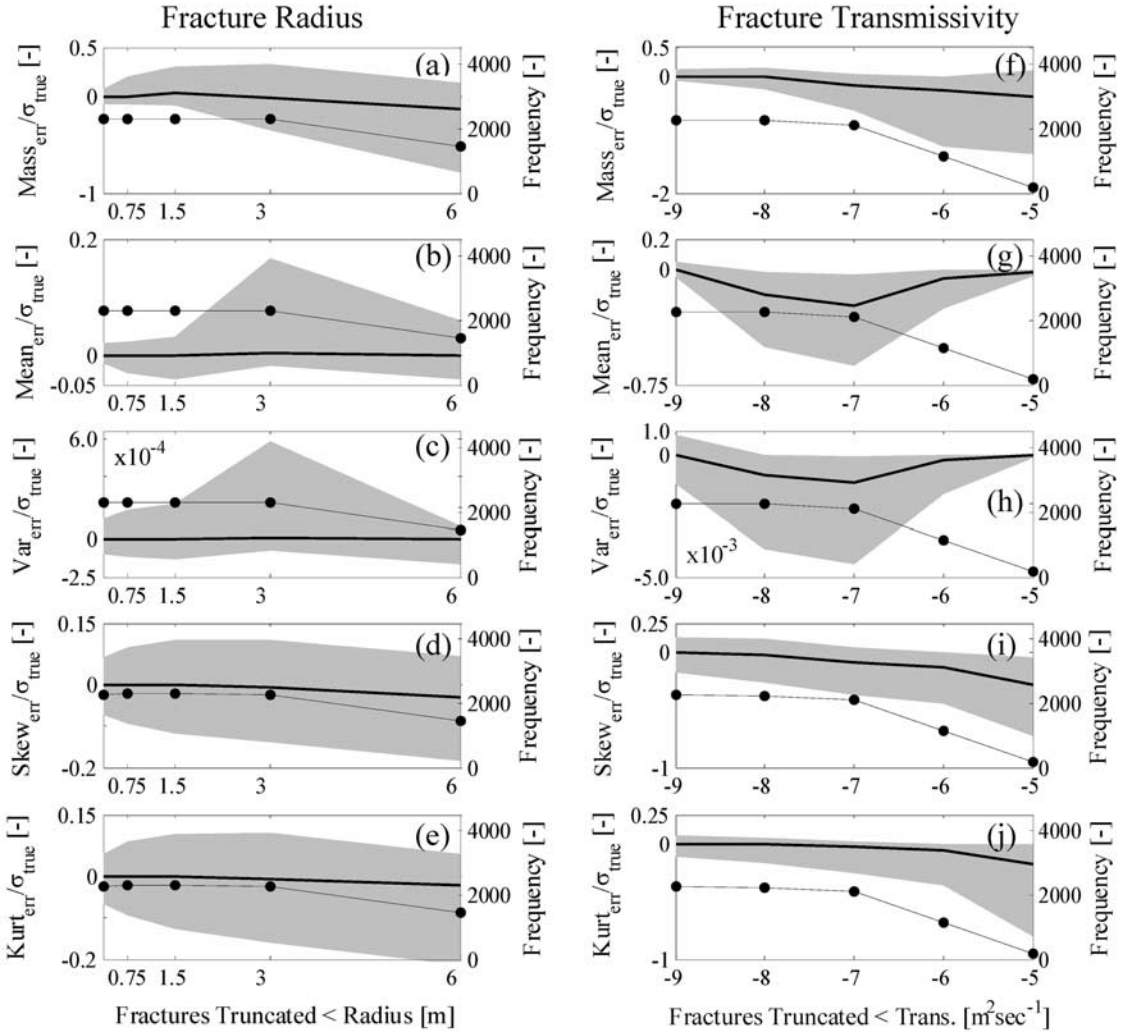

Figure 5. Moment error is normalized by the standard deviation of the corresponding true moments (σ_{true}) for network simplification by fracture (a–e) radius and (f–j) transmissivity in the 'X' direction (Figure 1a). Rows distinguish the prediction error in the mass, mean, variance, skewness, and kurtosis from top to bottom, respectively. The dark lines indicate the median error bounded by the 25th to 75th percentiles in gray associated to values on the left plot axis. The *x* axis indicates the threshold below which features are removed during network simplification. The right plot axis is associated to the lines with dots, and gives the number of cases that are present at each level of network simplification, which is identical by column.

cation causes substantial variability in error magnitude at most levels of network simplification for all moments except variance, which exhibits a value range of nearly nine orders in magnitude, and (4) when comparing the results of constant frequency the range of prediction error generally increases with greater simplification of the network.

3.4. Enhanced and Restricted Transport

[32] A conceptually interesting and perhaps unintuitive response from network simplification is that prediction error may be positive or negative (Figure 5). In accordance to the classic advection-dispersion equation removing 'micro' fractures should lessen diffusion and dispersion (variance), and increase mean flow velocity. This analysis partially supports this paradigm but also shows that the opposite effects may occur. Particles may travel faster because of network simplification, which can occur when low-velocity flow regions are eliminated from the network and there is little disruption to the primary pathways controlling solute migration toward the location evaluated. Conversely, the elimination of fractures may slow particles if the removed fractures eliminate key hydraulic pathways and the alternative flow routes have slower velocities, or are more tortuous, such that the overall arrival time is lengthened. This concept is visually illustrated in Figure 6. Fracture network simplification can alter primary hydraulic pathways controlling solute migration, reroute solute travel along different flow directions, and change the proportion of mass that is trapped within low-velocity flow zones.

[33] The sign of the moment error caused by fracture network simplification implies that transport is either "restricted" or "enhanced." Using the same convection as above, a positive error for the mean arrival implies that transport is "restricted" because the average arrival time is prolonged by network simplification. A positive error for the mass

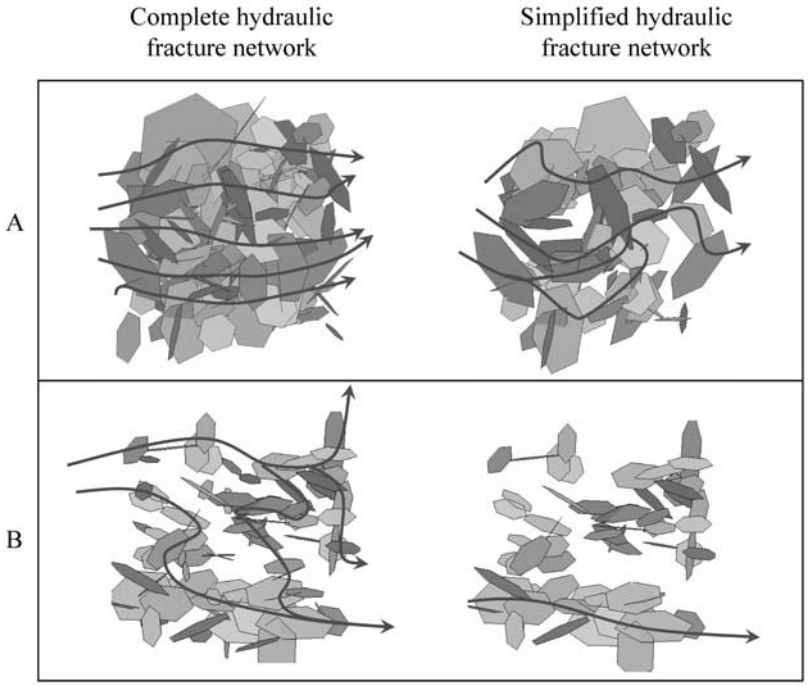

Figure 6. A conceptual illustration of enhanced and restricted transport caused by fracture network simplification, as defined in the text. (a) Network simplification causes an increase in dispersion and a decrease in mean velocity. (b) Network simplification causes a decrease in dispersion and an increase in mean velocity.

arrival indicates that transport is "enhanced" since more solute migrates through the structurally simplified network than in the complete hydraulic network in the time evaluated. For the presented breakthrough curves, network simplification in the "small" fracture network leads to enhanced behavior in mean arrival time. For the "medium" fracture network transport is mainly restricted (Figure 4, top row). Interestingly, for minor amounts of network simplification (< 0.375 m radius) in the "small" network at 32 m of travel, particle migration is slowed and less mass propagates within the primary plume, but as additional fractures are removed (< 1.5 m radius) the plume once again moves faster along the "X" coordinate direction near the average velocity of the complete ("truth") network (Figure 4, bottom left). In this case, a small amount of network simplification reduces pathways along the "X" coordinate direction, and some of the secondary pathways in the original network become new primary pathways in the simplified network, diverting particle migration in alternative directions such that mass is prevented from reaching the observation location. With additional network simplification the hydraulic pathways are further altered, which limits the diversion of solute in alternate directions and again renders the primary plume migration mainly along the "X" coordinate direction. The type of behavior that occurs in a specific instance is conceptualized as the balance between forces that promote or delay solute migration across defined regions in an aquifer.

[34] The cases of restricted and enhanced transport are evaluated in relation to three fracture network attributes (i.e., fracture surface density, maximum fracture radius, power length exponent) and the distance from injection. The goal is to understand when enhanced and restricted transport occur most frequently. Results from the 2510 (2780 – 270 base) simplified models and nine observation locations collinear to the hydraulic gradient (Figure 1; 'X' direction) are considered. The largest positive and negative errors are selected for evaluation using the upper and lower quartiles of the error distribution, which avoids the ambiguous circumstance where error magnitude is near zero and unimportant. A measure of relative occurrence is used in the form

$$P(\chi|\omega) \cdot P(\chi)^{-1}, \tag{7}$$

where *P()* is the probability, χ is a condition of enhanced or restricted transport, and ω represents one of the three network attributes or distance from source injection. The first term is the conditional probability that transport is enhanced or restricted given a specified value of the attribute considered, and is normalized by the probability that the same condition occurs for all values of that property. If the probability for a given parameter value is equal to the probability for all values, then the ratio of equation (7) will be unity (one). A relative occurrence close to one implies that an attribute value has little influence on whether transport is enhanced or restricted. A relative occurrence that is greater or less than one implies there is an increased or reduced probability, respectively, that a particular behavior will occur given a particular attribute value.

[35] The mass arrival results using relative occurrence are first examined (Figures 7a–7d). For the bulk P_{32} density there is little influence in either the enhanced or restricted behavior (Figure 7a). The most notable pattern is when transitioning from a P_{32} density of 1.0 to 2.5 where the

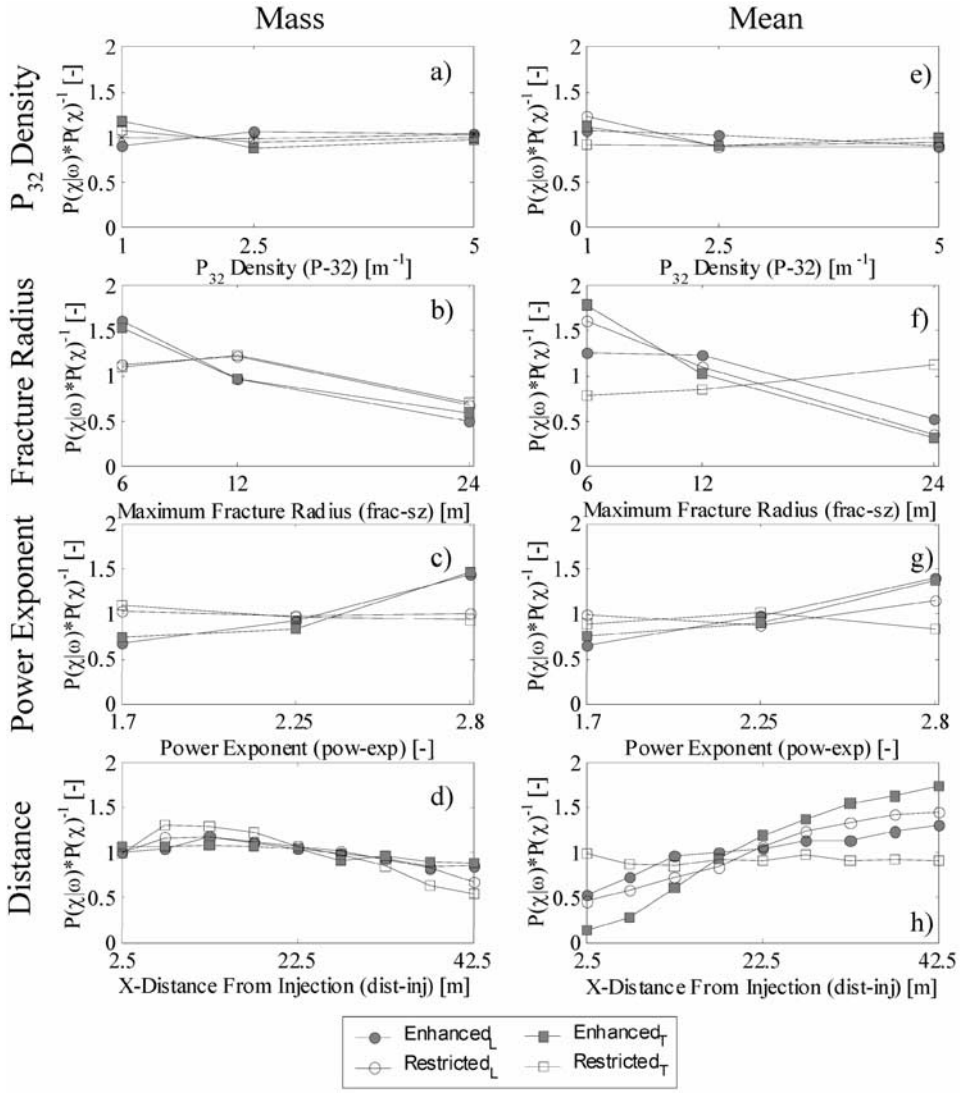

Figure 7. The ratio of observed enhanced and restricted transport for each attribute to statistical expectation from random selection (*y* axis) versus each attribute value (*x* axis), as described in the text. Legend subscripts "T" and "L" refer to network simplification by fracture transmissivity and radius, respectively.

enhanced conditions decrease and the restricted conditions increase. Overall, the influence of bulk fracture density on enhanced or restricted transport is minimal.

[36] The largest fracture (maximum radius) in a network negatively influences relative occurrence (Figure 7b). The relative occurrence for enhanced transport is high when the largest fractures in a network are relatively small (6 m), randomly expected when moderately sized (12 m), and low when relatively large (24 m). This suggests that enhanced transport occurs more frequently when the elimination of fractures eliminates some of the trapping mechanisms within the network while still allowing for adequate flow through mainly small-scale pathways. If large-scale fractures are present they tend to control connectivity and transport across the network. In the latter case, removing the background fractures will less frequently lead to enhanced transport conditions because few (if any) of the primary transport paths are largely affected. For the restricted transport conditions, there is also a lower relative occurrence for a maximum fracture radius of 24 m, implying the same processes are present. At 6 m, however, the relative occurrence of restricted transport is near one, which indicates that smaller fractures do not influence restricted transport. Enhanced transport is influenced substantially when small fractures are present in the network. The strongest effects in relative occurrence occur for enhanced transport.

[37] The power length exponent has appreciably different effects on enhanced and restricted transport (Figure 7c). Given that a small power exponent typically leads to large-sized fracture populations, and vice versa, there is added support that networks with large fractures have a low relative occurrence of enhanced transport and that those with small fractures have a high relative occurrence. However, because the relative occurrence of restricted transport is near unity (one) for all distributions, the fracture length distribution of the network is presumed less influential in restricting pathways than the largest feature in the network (maximum fracture radius).

[38] The influence of travel distance from the injection source on enhanced and restricted transport is examined (Figure 7d). Relative occurrence increases for particle travel near the source injection and decreases with travel to greater distances, primarily for restricted transport. Two processes become evident. First, the networks that show greater restricted transport near the source injection can be different from those that show less restricted transport at greater distances. This is because networks with higher connectivity allow for particle migration to the greatest travel distances and are not necessarily restricted near the source injection region. The networks that do promote restricted transport near the source injection may not possess sufficiently connected pathways for migration across the entire region and therefore do not affect the results at the greatest distances examined. Second, there may be offsetting influences with increasing plume travel. As a result of network simplification some of the connections to the primary flow channels may be eliminated, which may restrict transport near the source injection region. Once particles are ultimately mobilized into primary flow channels there is a greater tendency for the particles to stay within primary channels than in the complete network because network simplification removes some of the low flow pathways that restrict particles and possibly a portion of the secondary channels that cause particles to exit through the lateral edges of the model. Thus, too many particles may be restricted near the source because of network simplification, but with greater travel distances too few may be retarded or exit the domain such that the effects begin to offset one another at intermediate distances. There is no indication from this analysis that a perfect balancing of offsetting influences will occur, so it is expected that some residual effect will be present be it small or large in magnitude.

[39] The relative occurrence of the mean arrival error (Figures 7e–7h) is evaluated for the same attributes and compared to the results for mass arrival, described above (Figures 7a–7d). There is general agreement between the mass and mean analyses of relative occurrence as a function of the fracture density, maximum fracture radius, and power exponent. A clear exception to this is restricted transport as a function of maximum fracture radius when simplifying by transmissivity (Figure 7f). Direct investigation suggests that the difference in behavior is due to negative median values for the mean arrival error at three of the five levels of network simplification (Figure 5g, 10^{-8}, 10^{-7}, and 10^{-6} m^2 s^{-1}). There is also a similar effect in the relative occurrence for the enhanced transport when simplifying by transmissivity. Excluding these nonzero median values, enhanced and restricted transport show a lower relative occurrence at short travel distances and greater relative occurrence at larger distances when considering the mean arrival time. The pattern of relative occurrence for the mean arrival is therefore opposite to the results for the mass arrival.

[40] Direct investigation of the results shows there are exceptions in all of the observed behaviors. Despite this variation in behavior it is beneficial to discuss the general patterns that become apparent. The analysis shows that fracture network simplification generally causes chemical migration in networks with primarily small features to become enhanced in the mass and mean arrival and to lesser extent restricted in the mean arrival. This implies that more solute tends to propagate through a simplified network composed of "small" fractures than in the complete network in the time evaluated and at a higher average velocity. This behavior occurs when the flow pathways in the complete network that divert particles out of the domain prior to reaching an observation location or act to retard migration in low-velocity zones are eliminated during network simplification. If there are dominant fractures present in the network they tend to control transport, and both restricted and enhanced transport conditions occur less frequently when the network is simplified. Moreover, these influences on transport may not be correlated to one another. For example, the strongest enhanced conditions for the mean arrival occur when the maximum fracture radius is small, power exponent is large, and the farthest travel distance is reached. For the same fracture network at short travel distances there is the tendency to limit enhanced conditions which counteracts the effects of the network attributes. Thus, it appears that multiple attributes jointly influence how transport is affected. Attributes may collectively promote a single effect or may oppose one another such that a balance of effects determines the observed outcome.

3.5. Multivariate Regression Analysis

[41] To examine how multiple attributes simultaneously correlate to the transport prediction error caused by network simplification, a multivariate linear regression strategy is adopted that relates moment error (μ_{error}) to the measured attributes (ψ) through a set of coefficients (a) as given by

$$\left|\frac{\boldsymbol{\mu}_{error}}{\mu_\sigma}\right| = \left[a_0 + \sum_{i=1}^{N} a_i \cdot \frac{\psi_i}{\psi_\sigma}\right] + \boldsymbol{\xi}. \tag{8}$$

The moment errors (i.e., mass, mean, variance, skewness, and kurtosis arrival errors) are related to the combined effect from N attributes (i.e., fracture density, maximum fracture size, power length exponent, distance from injection, and level of network simplification). Both terms are normalized by their respective standard deviations (σ) to nondimensionalize values and equate distribution variances. All errors and attributes are evaluated in their true form with the exception of variance which undergoes a $\log_{10}$ transformation. The residual term (ξ) is minimized using the sum of squared residuals

$$\boldsymbol{\xi}'\boldsymbol{\xi} = (\boldsymbol{\mu}_n - \boldsymbol{\psi}_n\mathbf{a})^T(\boldsymbol{\mu}_n - \boldsymbol{\psi}_n\mathbf{a}). \tag{9}$$

The derivative of equation (9) is set to zero and solved in terms of the regression coefficients in the least squares form

$$\hat{\mathbf{a}} = \left(\boldsymbol{\psi}_n^T\boldsymbol{\psi}_n\right)^{-1}\left(\boldsymbol{\psi}_n^T\boldsymbol{\mu}_n\right), \tag{10}$$

with $\boldsymbol{\mu}_n = \left|\frac{\boldsymbol{\mu}_{error}}{\mu_\sigma}\right|$ and $\boldsymbol{\psi}_n = \frac{\boldsymbol{\psi}}{\psi_\sigma}$ [e.g., *Lawson and Hanson*, 1974]. The resulting coefficients ($\hat{\mathbf{a}}$) indicate the relative influence of an attribute on moment error, and the sign of the coefficient indicates a positive or negative correlation.

[42] The regression coefficients are evaluated with respect to their statistical significance using the p-value method that is discussed in most statistical texts. The p-value is the probability of obtaining a t-statistic at least as extreme as

Table 3. An Example Multivariate Analysis for Evaluating the Correlation of "Attributes" to Moment Prediction Error[a]

Regression Statistics	Value					
Multiple R	0.60					
R Square	0.36					
Adj. R Square	0.36					
Standard Error	0.81					
Observations	10632					
Dimensionless Attributes	Coefficients	Standard Error	T Statistic	P Value	Lower 95%	Upper 95%
Fracture Density (P-32)	−0.03	0.01	−3.98	0.00	−0.04	−0.02
Maximum Fracture Radius (Frac-Sz)	−0.18	0.01	−24.50	0.00	−0.20	−0.17
Power length Exponent (Pow-Exp)	0.14	0.00	31.69	0.00	0.13	0.15
Network Simplification (Trunc)	0.34	0.01	43.43	0.00	0.33	0.36
Travel Distance (Dist-Inj)	−0.13	0.01	−17.05	0.00	−0.14	−0.11

[a]All quantities are dimensionless.

the one in question through random selection. The procedure is to estimate regression coefficients and set the insignificant terms ($p > 0.05$) to zero. Three data sets (i.e., 'All', 'Enhanced', and 'Restricted') as determined by the mean arrival time of particles are examined for their error relations. A separate analysis is performed for each temporal moment along the "X" and "Y" coordinate directions (i.e., collinear and orthogonal to the hydraulic gradient). In all, 60 multivariate regression analyses are conducted using the 2780 models and 15 observation locations (e.g., one example in Table 3).

[43] It is first recognized that the results using the three data sets (top, middle, and bottom rows) for transport in the "X" coordinate direction are relatively similar (Figure 8). The same is true for transport along the "Y" coordinate direction and for brevity graphical presentation is restricted to the "All" data set for the "Y" direction (Figure 9). Further comparison between the coefficients for transport along the "X" and "Y" coordinate directions also shows moderate agreement. A notable exception is less influence by travel distance on the mean and variance of particle arrival in the "Y" direction. This is attributed to the majority of flow paths collinear to the hydraulic gradient. Additional comparison between network simplification by fracture radius (Figures 8a–8c) and fracture transmissivity (Figures 8d–8f) indicate general similarity. A key difference is a greater influence when simplifying the network by fracture radius for the cases examined. Overall, the differences between flow direction, method of network simplification, and data set are shown less substantial than the variability between the examined attributes (i.e., between fracture density, power length exponent, maximum fracture size, degree of network simplification, and travel distance from source injection). Discussion is therefore focused on the differences between attributes, and specifically on the results for the "All" data set in the "X" direction when simplifying a network by fracture radius (Figure 8a).

[44] The errors in predicting the mass arrival of particles and the mean and variance of particle arrival times crossing the observation polygons are influenced by each attribute considered. Higher-order moments (skewness and kurtosis) are mainly affected by the plume travel distance. Network simplification is positively related to moment error, which is expected given that it is the source of error in this investigation, but the attributes of the fracture network and plume travel distance exhibit comparable relations to the observed error. Thus, to explain the moment error resulting from fracture network simplification, the level of network simplification, network attributes, and travel distance should be considered.

[45] In the interest of brevity, the influence of each attribute on moment error is discussed in a general context. Subtle relations can be viewed through direct examination of the results. The maximum fracture size ("Frac-Sz") shows an inverse relation to moment error, which suggests that networks with large features have greater connectivity and that less error will result from network simplification when dominant features are present. The effect of the maximum fracture size is most pronounced when predicting the mass, mean, and variance of particle arrival at the defined observation locations. For the power length exponent ("Power") there is a positive relation to all moment error, further supporting that when fractures in a network are relatively small (large exponent value) there are larger errors caused by network simplification, and when dominant features exist (small exponent value) the error from network simplification is generally less. The correlation of the P_{32} fracture density ("P-32") is either insubstantial or reveals a negative relation to fracture network simplification. The strongest effect from fracture density is the negative relation to error in the mean and variance of particle arrival, which implies that network simplification of dense fracture networks leads to relatively low error when predicting the advection and dispersion of solute as compared to simplification of sparse networks. However, for the mass arrival of particles, and skewness and kurtosis of particle arrival time error there is no such relation. For greater plume travel, the mass and higher-order moment error tends to decrease while the error in predicting the mean and variance of particle arrival tends to increase.

[46] As a synopsis, the multivariate regression analysis provides an estimate of how multiple attributes jointly affect the error in transport predictions caused by fracture network simplification. Linear regression coefficients reveal general tendencies as there are no conditions where a single behavior will always occur. The variation in coefficient magnitude of the moments examined indicates that error is a function of the metric used for evaluating transport. The error in predicting the mass arrival of particles, and mean and variance of particle arrival times is affected by all of the attributes examined, while the higher-order errors are mainly influenced by the plume travel distance. Dense networks

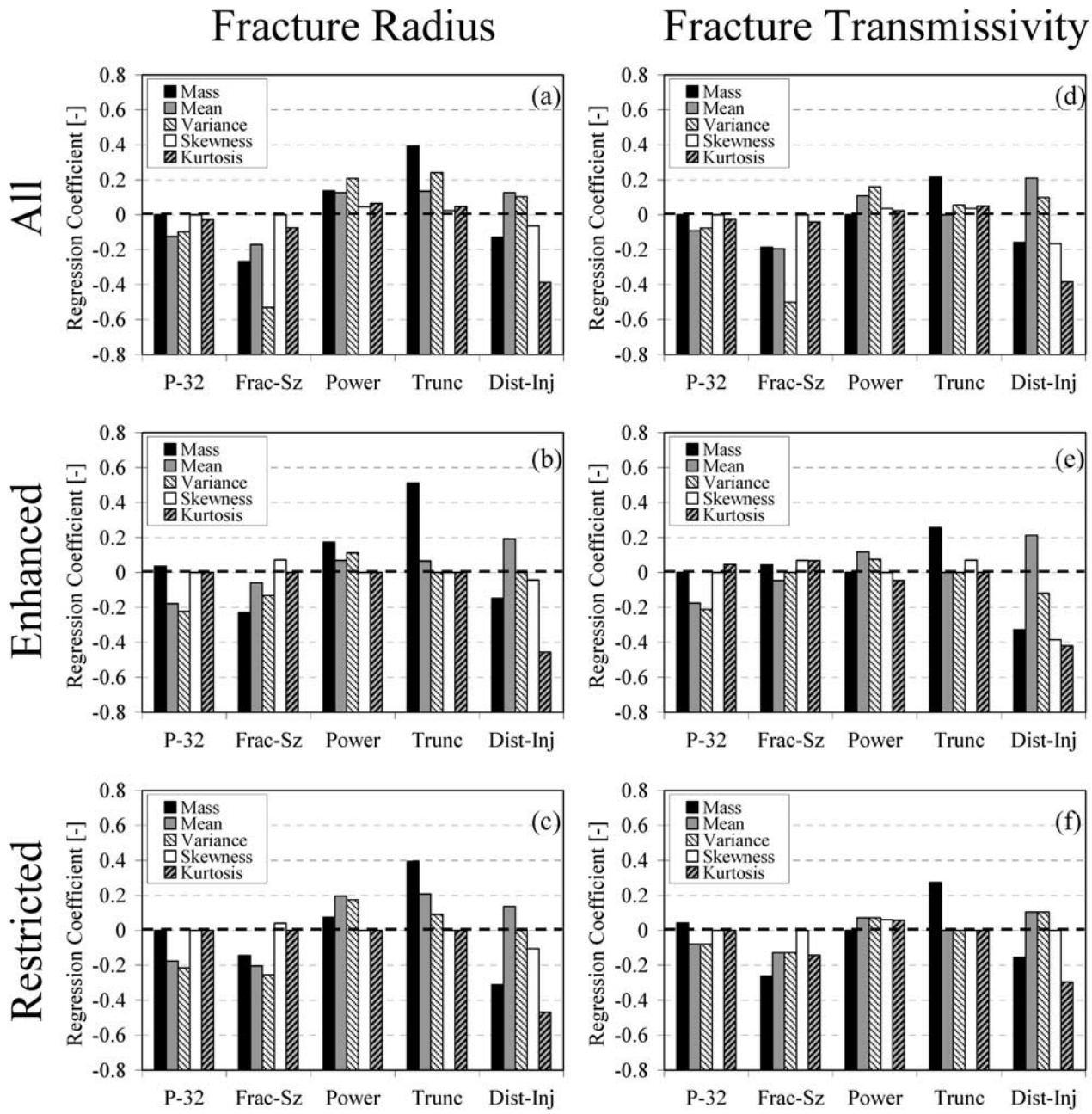

Figure 8. Multivariate regression analyses collinear to the hydraulic gradient (see Figure 1a, 'X') for network simplification by fracture (a–c) radius and (d–f) transmissivity. Rows distinguish the relations between the different data sets (i.e., all errors, enhanced cases (lowest 25% of errors), and restricted cases (highest 25% of errors), as determined by the mean arrival). A positive coefficient indicates a positive correlation to network simplification error, and vice versa. 'P-32' ≡ fracture density, 'Frac-Sz' ≡ maximum fracture size, 'Power' ≡ power length exponent, 'Trunc' ≡ degree of network simplification, "Dist-Inj" ≡ distance from injection.

tend to exhibit less error for the mean and variance of arrival as compared to sparse networks, but there is no such relation for the remaining moment measures. Networks with dominant fractures tend to be less affected by network simplification as compared to networks composed of small fractures due to their control on connectivity. With larger travel distance the prediction errors in the mean and variance of arrival time tend to increase while those for the mass arrival, and skewness and kurtosis of arrival time errors tend to decrease. Greater amounts of network simplification tend to increase prediction error in the mass arrival of particles, and mean and variance of particle arrival times, but there is no significant trend identified for the skewness and kurtosis. Combining the latter with previous results in section 3.2 suggests that while plumes with greater complexity have larger percentages of error relative to the moment magnitude the amount of structure removed from a network will not necessarily dictate the magnitude

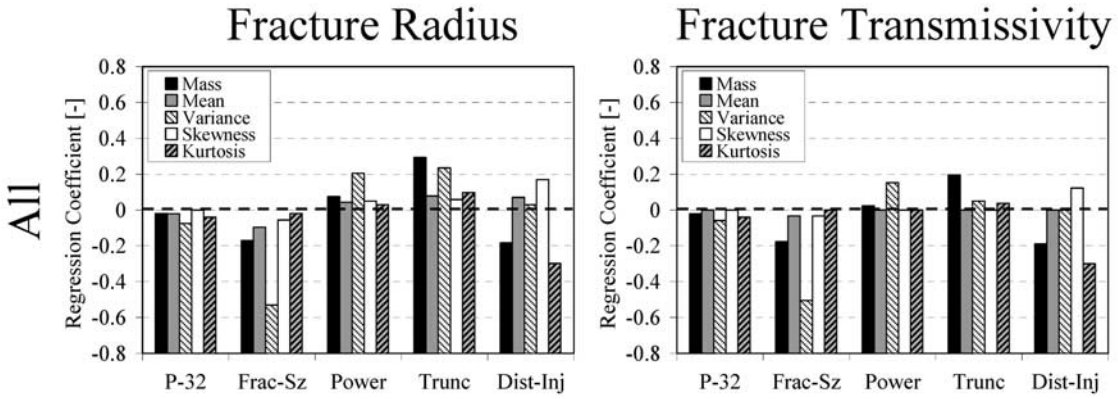

Figure 9. Same as Figure 7 for the "all" data set, except that transport is orthogonal to the hydraulic gradient ('Y' direction, Figure 1a).

of moment error for the higher-order moments. Overall, the maximum fracture size, distance from injection, and level of network simplification have the strongest influences on moment prediction. Lesser effects are found for the power length exponent and bulk fracture density. In general, there is a measurable influence by all attributes examined on the error in predicting transport caused by network simplification.

3.6. Prediction Error as a Random Process

[47] The probability of encountering error is determined by the proportion of models with error below a specified value (Figure 10). The resulting cumulative error distributions derived through the analog models used in this investigation are a proxy to the effect of using a simplified model over one constructed with the actual fracture network structure of an aquifer. The results reveal that the level of error (i.e., 1, 10, and 50%) and the moment considered strongly influence the percentage of models that are deemed permissible. When predicting the mass arrival of particles or mean particle arrival time there is an $\sim$80–90% probability that error is below 50%, and a $\sim$30–60% probability that error is less than 10%. This suggests that estimates of the mass arrival of particles and mean arrival time of particles are relatively forgiving to moderate amounts of network simplification. However, for the variance, skewness, and kurtosis of particle arrival times there is only a $\sim$40–60% probability that prediction error is less than 50%, and a $\sim$15% probability that errors will fall below 10%. Given that the variance, skewness, and kurtosis moments are known to reflect critical transport characteristics in heterogeneous systems, these higher order effects are considered of greatest relevance. This is especially true where contaminant toxicity is high and the plume's tailing edge is an important consideration for remediation efforts. Moreover, these estimates do not consider the error from eliminating fractures below a 0.3 m radius, using a minimum transmissivity value of 1×10^{-10} m^2 s^{-1}, or ignoring important "matrix" processes. Collectively, the results suggests that it is often insufficient to create a single structurally simplified model using only the 'substantial' fractures even if the represented features are perfectly characterized. To make individual simplified models accurate a compensating effect must be combined to the perfectly characterized fractures in the network to offset the effects of those ignored. Given that

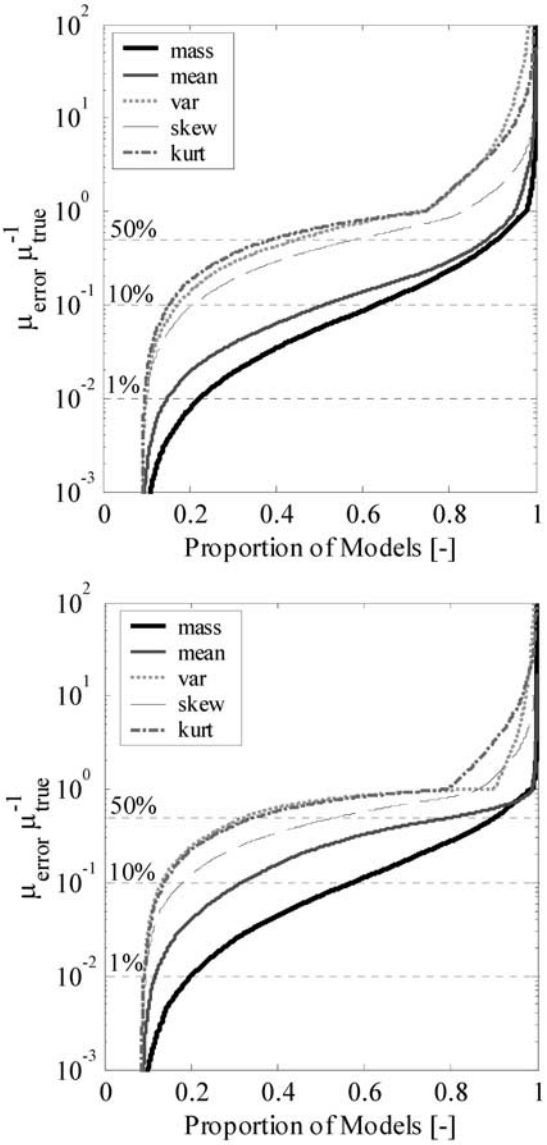

Figure 10. Absolute temporal moment error normalized to true values (i.e., |simplified - true|/true) and sorted by magnitude for networks simplified by fracture (top) radius and (bottom) transmissivity. Horizontal lines correspond to 1, 10, and 50% error.

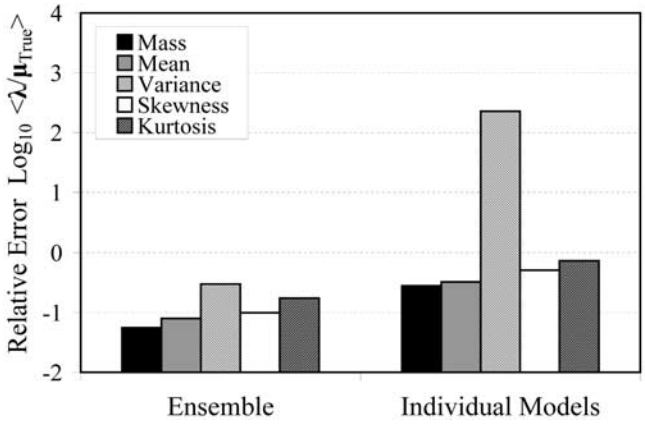

Figure 11. Comparison of the average absolute individual model error and the average absolute median error of each ensemble. The residual term (λ) for the individual models is $|\mu_{\mathbf{i}}-\mu_{\mathbf{true}}|$ and for each ensemble of models is $|\text{median}(\mu_{\mathbf{i}},-\mu_{\mathbf{true}})|$. Note that relative error is in $\log_{10}$ scale.

network simplification may cause both positive and negative errors for the moments examined, the compensating function should be capable of properly reducing or increasing solute dispersion predicted by the explicitly modeled portion of the fracture network, as opposed to being invariantly additive to mean advection as predicted by the classic ADE. More generally, however, all predicted moment behaviors using a simplified model must be simultaneously corrected in three-dimensions for all space and time.

3.7. Ensemble Averaging

[48] Given the limited ability of individual simplified models in predicting transport processes accurately, an error reduction strategy is evaluated using ensemble-averaged predictions from the 27 suites (i.e., parameter combinations) of models evaluated in this study. Separate analyses are used to determine the expected error from each ensemble of models, expected error in individual models, and model error in relation to the variability of predictions inherent to a stochastic description of the fracture network. The latter measure is an indication of the range of predictions that result when a fracture network is described probabilistically, which is often the case because fractures may be mapped either at the land surface or in well-bores to attain bulk attribute distributions, but the majority of in situ subsurface features cannot be measured.

[49] The average relative error for an ensemble of models is given in the form

$$\left\langle \left| median\left(\left\{ \frac{X_{i,j,k,d} - (X_{true})_{i,k,d}}{(X_{true})_{i,k,d}} ; i = 1, \ldots n_{real} \right\} \right) \right| \right\rangle_{j,k,d} \quad (11)$$

where $X_{i,j,k,d}$ is a predicted moment for a given realization i (1 to 10), level of network simplification by fracture radius j (1 to 5), parameter combination k (1 to 27), and observation distance d (1 to 9) along the "X" direction, and $(X_{true})_{i,k,d}$, is the "true" moment determined from the corresponding original (nonsimplified) "true" fracture network model. The median of each ensemble is used in lieu of an arithmetic mean to achieve lower effective error because of the skewed error distributions identified in this analysis (Figure 5). The median term on the LHS of equation (11) is the absolute relative error determined for each set of realizations corresponding to a particular level of network simplification, parameter combination, and travel distance. The expected value is calculated for all median error terms. The resulting expected relative error is the average ratio of the ensemble error from each suite of models normalized by the "true" moments. The same calculation is performed for all moments. Results indicate that the expected relative errors for the mean and variance of particle arrival are 0.1 and 0.5, respectively.

[50] The relative error in using a single model is estimated by

$$\left\langle \left| \frac{\langle X_{true} \rangle_{k,d} - (X_{true*})_{i,k,d}}{\langle X_{true} \rangle_{k,d}} \right| \right\rangle_{i,k,d} \quad (12)$$

where $\langle X_{true} \rangle_{k,d}$ is the expected value from the ensemble of "true" models that is assumed to be the "truth," and $(X_{true*})_{i,k,d}$ is a random selection from the ensemble of "true" models that represents the single model. The relative error for a single model is then approximated as the expected ratio of the prediction error to the "true" moment value. This result is interpreted as the error in using a single model for transport prediction. Results indicate that the mean and variance of particle arrival times are approximately 0.50 and 1.1, respectively, with a variation of up to ±0.1 depending on the random selection of the individual model.

[51] A measure of the variability using a suite of stochastically described fracture network models is estimated by the coefficient of variation in the form

$$\left\langle \left(\frac{\left(\left\langle (X_{true})_{i,k,d} - \langle X_{true} \rangle_{k,d} \right\rangle^2 \right)^{0.5}}{\langle X_{true} \rangle_{k,d}} \right) \right\rangle_{i,k,d}, \quad (13)$$

which is a measure of the dispersion in the probability distribution. Equation (13) may be interpreted as the expected variability between moments in the ensemble compared to the average predicted moment, or in other words how the predictions of stochastic models vary from one another. As with equations (11) and (12) this is a relative measure normalized to the "truth." Results indicate that the expected coefficient of variation for the mean and variance of particle arrival is 0.7 and 1.8, respectively.

[52] The analyses reveal that the ensemble error in the mean and variance of particle arrival is, on average, 80 and 55% less, respectively, than the error inherent to single models, and on average, 85 and 70% less, respectively, than the range of predictions in describing the fracture network stochastically. As an additional analysis, the ensemble error is compared to the average individual model error (Figure 11). Results indicate that the ensemble error for the mass, mean, variance, skewness, and kurtosis of arrival is, on average, 80, 75, 99, 80, and 76% less than the average error per model. The median ensemble prediction from a suite of simplified fracture network models is shown to provide a

reasonable estimate of transport processes with substantially less error, on average, than individual models.

[53] To further examine average characteristics of the total sample set, moment errors are analyzed as a function of the fracture density, power length exponent, and degree of network simplification (Figure 12). Errors are given as percentages normalized to the corresponding ''true'' moments (i.e., |predicted-true|*100/true). General patterns are readily apparent when averaging over ten realizations, three maximum fracture sizes, and nine evaluated distances along the ''X'' coordinate direction. The patterns are greater error caused by network simplification for fracture networks with lower fracture density and larger power exponents, and those which have undergone greater amounts of simplification. The patterns of error are roughly consistent for the mass, mean, and variance of particle arrival. An exception being that the mass error has little relation to fracture density, as was indicated in the multivariate analyses above. For higher moments error patterns are less apparent. Errors range mainly between 15 and 70% of the ''true'' moment values and tend to increase with increasing moment order.

4. Final Remarks

[54] The range of fracture network parameters evaluated in this investigation is limited to 27 unique combination sets and 10 realizations per combination. The range of conditions accounts for a portion of the expected variability of transport behavior in fractured aquifers. Limiting parameter combinations and realizations is necessary to restrict the number of models to a tractable level. A systematic procedure is developed for eliminating increasing amounts of structure from 270 base fracture networks, thereby creating 2780 models that are used to evaluate the effects of network simplification on transport processes. The influence of using limited realizations is diminished by examining transport at 15 locations throughout the model domain and by calculations that employ multiple parameters sets. However, some parameter variability is not considered. Given this issue of incomplete parameter variability as well as simplified model representation that ignores fracture microstructure, the results of this investigation are viewed as minimum estimates of the effects of simplifying fracture network representation on inert chemical migration in fracture-controlled aquifers.

[55] Despite these limitations, this investigation is beneficial in addressing a fundamental issue in fractured-rock hydrology. It is determined which fractures within a network of fractures impose a substantial control on chemical migration. The results suggest that a fracture's individual properties such as size, conductance, orientation, and porosity can affect the level of its control on chemical migration. The surrounding network in which a fracture is integrated further affects its ability to control transport. A fracture's influence on transport may evolve with increased plume travel from the injection source, and may change depending on the transport measure that is considered. Ignoring a portion of the fracture structure in the model representation can lead to prediction error that is small to large in magnitude for most cases examined, but under no set of circumstances is the error caused by ignoring fracture structure invariably minor except as the level of network simplification and time from injection approach zero. Even

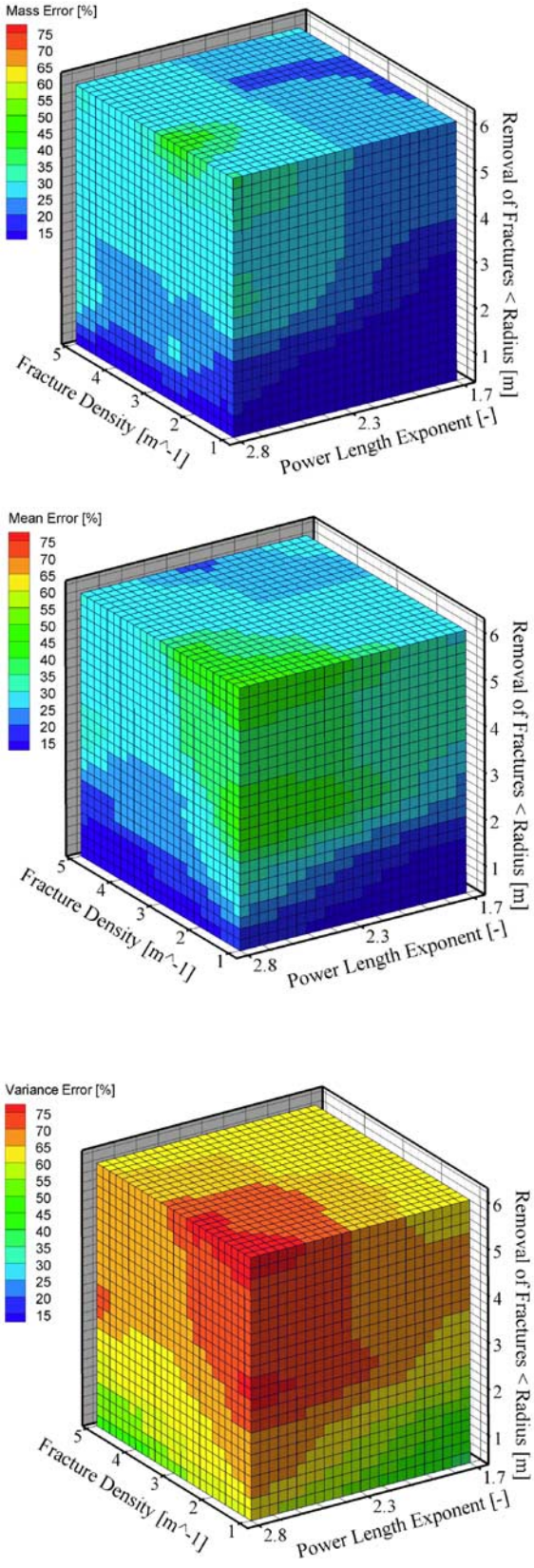

Figure 12. Average error percent [|moment error|*100/true moment] that is caused by fracture network simplification for the mass, mean, and variance of particle arrivals as a function of the fracture density, power length exponent, and degree of network simplification for transport along the ''X'' coordinate direction (Figure 1a).

for fracture networks with large dominant fractures there are some, albeit fewer, instances where prediction error is relatively large. Analyses show that approximately 50% of the simplified networks examined lead to greater than 50% error in the prediction of higher-order plume characteristics. This suggests that the effects of network simplification should not be ignored. Using the median ensemble prediction from a suite of structurally simplified models is the most effective means of minimizing error that is identified in this analysis. On average, ensemble predictions have at least 50% less error than individual models and at least 70% less error than the variability of predictions from characterizing the fracture network stochastically.

[56] Several interesting effects result from fracture network simplification. Network simplification can change the primary hydraulic pathways controlling solute migration, re-route solute travel along alternate network channels, and alter the proportion of mass retarded within low-velocity flow zones. The net effect of these influences distinguishes whether 'enhanced' or 'restricted' transport will occur as a result of fracture network simplification. Enhanced transport in the mean particle arrival time occurs when solute trapping mechanisms are reduced and there is little disruption to the primary pathways controlling solute migration. Conversely, restricted transport of the mean particle arrival is conceptualized where the elimination of fractures affects critical linkages such that hydraulic pathways are substantially altered, and transport particles are either diverted along alternate flow paths in different directions or retarded within low-velocity flow regions, thus slowing plume movement. In all, simplifying the fracture network structure may cause solute particles to propagate farther, faster, and to exhibit greater dispersion and tailing than will occur in the complete fracture network. Alternatively, opposite effects may occur for some or all of these behaviors for a given circumstance. The implications of enhanced and restricted transport challenge traditional models. Predictions using a simplified network representation can exhibit greater variance in the solute arrival as compared to the complete network. If a separate function is selected to compensate for the effect of the removed features, such as a dispersion function, the function must reduce solute mixing through the simplified fracture network rather than increase it, contrary to the classic advection-dispersion equation where the effects of the ignored microfeatures are invariably additive to the mean flow. Although the separation of the fracture network structure into an explicitly modeled component and a secondary function is traditionally viewed as a simplification the effects from such an approach appear to be rather complex.

[57] While it is expected that under changing fracture network characteristics, parameterization, support scale, and metric used to evaluate transport that the significance of network simplification will vary, enhanced and restricted conditions are hypothesized as generally applicable to a range of systems. Anecdotal evidence from the scale similarity of fracture network architecture and tailing in tracer measurements suggest that the results presented herein are relevant across a range of length scales, but universality of the identified effects is not established. For fracture networks that are self-similar in nature the results of this study could offer scaled analogs of processes at larger scales. In the event that the characteristic length of the fracture network connectivity is less than 1/10 to 1/5 of the support scale examined there is perhaps sufficient averaging such that the effect of network simplification is sufficiently minimized [*Molz et al.*, 2004]. Synthetic studies of fracture networks, however, suggest that network connectivity may be nonasymptotic under certain circumstances [e.g., *Bour and Davy*, 1998]. Additional support for large scale influence is evident from the examination of scales for predicting bulk fluid flow in fractured aquifers applicable to evaluating water resources, which shows that basin scale consistency in fluid behavior is not reached until $\sim$100 m–1000 m [*Wellman and Poeter*, 2005, 2006]. This implies that sufficient averaging of transport processes will occur at larger length scales given its greater dependence on flow path variability. In light of these points and readily observable large-scale heterogeneities from direct observation that control regional flow (e.g., faults) there remain valid questions as to whether the effects presented herein eventually diminish. Scale relations deserve additional attention beyond that provided in this investigation.

[58] **Acknowledgments.** The first author wishes to thank the U.S. Geological Survey for enabling this project through a National Academies postdoctoral fellowship. Two anonymous reviewers and Jean-Raynald de Dreuzy provided excellent comments that improved this paper significantly. Their efforts are sincerely appreciated. Internal USGS reviews by Paul Hsieh and Fred Day-Lewis were also paramount in the improvement of this work. In addition, Brian Berkowitz is thanked for his role as editor for this paper. The authors wish to convey their gratitude to colleagues at Golder Associates, Inc., for permitting use of their FracMan software suite. It is emphasized that we have expressed our views and conclusions contained throughout this document, which should not be interpreted as necessarily representing the official policies, either expressed or implied, of our sponsors. Any use of trade, firm, or product names is for descriptive purposes only and does not imply endorsement by the U.S. Government.

References

Abelin, H., L. Birgersson, J. Gidlund, J. Moreno, I. Neretnieks, H. Widen, and T. Agren (1987), 3-D migration experiment, Report 3, Part 1, Performed experiments, results and evaluation, *Stripa Proj. Tech. Rep. 87-21*, Svensk Karnbransleforsoring, Stockholm.

Adler, P., and J. Thovert (1999), *Fractures and Fracture Networks*, 429 pp., Kluwer Acad., Dordrecht, Netherlands.

Andersson, J., L. Knight, and I. Staub (2005), Decovalex III/Benchpar projects, approaches to upscaling thermal-hydro-mechanical processes in a fractured rock mass and its significance for large-scale repository performance assessment summary of findings, report of BMT2/WP3, *SKB Rep., 2005:27*.

Andersson, P., J. Byegård, E. L. Tullborg, T. Doe, J. Hermanson, and A. Winberg (2004), In situ tracer tests to determine retention properties of a block-scale fracture network in granitic rock at the Äspö Hard Rock Laboratory, Sweden, *J. Contam. Hydrol.*, *70*, 271–297, doi:10.1016/j.jconhyd.2003.09.009.

Ando, K., A. Kostner, and S. P. Neuman (2003), Stochastic continuum modeling of flow and transport in a crystalline rock mass: Fanay-Augeres, France, revisited, *Hydrogeol. J.*, *11*(5), 521–535, doi:10.1007/s10040-003-0286-0.

Baecher, G. B., N. A. Lanney, and H. H. Einstein (1977), Statistical description of rock properties and sampling, in *Proceedings of the 18th U.S. Symposium on Rock Mechanics*, Am. Inst. of Mining Eng., Littleton, Colo.

Barton, C. A., M. D. Zoback, and D. Moos (1995), Fluid flow along potentially active faults in crystalline rock, *Geology*, *23*(8), 683–686, doi:10.1130/0091-7613(1995)023<0683:FFAPAF>2.3.CO;2.

Bear, J., C. Tsang, and G. de Marsily (1993), *Flow and Contaminant Transport in Fractured Rock*, 560 pp., Elsevier, New York.

Becker, M. W., and A. M. Shapiro (2000), Tracer transport in fractured crystalline rock: Evidence of nondiffusive breakthrough tailing, *Water Resour. Res.*, *36*(7), 1677–1686, doi:10.1029/2000WR900080.

Benson, D. A., S. W. Wheatcraft, and M. M. Meerschaert (2000), Application of a fractional advection-dispersion equation, *Water Resour. Res.*, *36*(6), 1403–1412, doi:10.1029/2000WR900031.

Berkowitz, B., and H. Scher (1995), On characterization of anomalous dispersion in porous and fractured media, *Water Resour. Res.*, *31*(6), 1461–1466, doi:10.1029/95WR00483.

Black, J., O. Olsson, J. Gale, and D. Holmes (1990), Site characterization and validation, Stage 4, Preliminary assessment and detail predictions, *Stripa Proj. Tech. Rep. 91-08*, 248 pp., Swed. Nucl. Fuel and Waste Manage. Co., Stockholm.

Bonnet, E., O. Bour, N. E. Odling, P. Davy, I. Main, P. Cowie, and B. Berkowitz (2001), Scaling of fracture systems in geologic media, *Rev. Geophys.*, *39*(3), 347–383, doi:10.1029/1999RG000074.

Bossong, C., J. Caine, D. Stannard, J. Flynn, M. Stevens, and J. Heiny-Dash (2003), Hydrologic conditions and assessment of water resources in the Turkey Creek Watershed, Jefferson County, Colorado, 1998–2001, *U.S. Geol. Surv. Open File Rep., 03-4034*, 148.

Bour, O., and P. Davy (1998), On the connectivity of three dimensional fault networks, *Water Resour. Res.*, *34*(10), 2611–2622, doi:10.1029/98WR01861.

Burton, W. C., J. G. Walsh, and R. Thomas (2000), Armstrong bedrock geologic map of the Hubbard Brook Experimental Forest, Grafton County, New Hampshire, *U.S. Geol. Surv. Open File*, *00-45*.

Cacas, M. C., E. Ledoux, G. de Marsily, B. Tillie, B. Barbreau, E. Durand, B. Fuega, and P. Peaudecerf (1990a), Modeling fracture flow with a stochastic DFN: Calibration and validation: 1. The flow model, *Water Resour. Res.*, *26*(3), 479–489.

Cacas, M. C., E. Ledoux, G. de Marsily, A. Barbreau, P. Calmels, B. Gaillard, and R. Margritta (1990b), Modeling fracture flow with a stochastic discrete fracture network: Calibration and validation 2. The Transport Model, *Water Resour. Res.*, *26*(3), 491–500.

Caine, J., and C. Forster (1999), Fault zone architecture and fluid flow: Insights from field data and numerical modeling, in *Faults and Subsurface Fluid Flow in the Shallow Crust*, edited by W. Haneberg et al., *Geophys. Monogr. Ser.*, *113*, 101–127, AGU, Washington, D. C.

Caine, J. S., and S. Tomusiak (2003), Brittle structures and their role in controlling porosity and permeability in a complex Precambrian crystalline-rock aquifer system in the Colorado Rocky Mountain Front Range, *Geol. Soc. Am. Bull.*, *115*, 1410–1424, doi:10.1130/B25088.1.

Caine, J., E. James, and C. Forster (1996), Fault zone architecture and permeability structure, *Geology*, *24*(11), 1025–1028, doi:10.1130/0091-7613(1996)024<1025:FZAAPS>2.3.CO;2.

Chiles, J., and G. de Marsily (1993), *Flow and Contaminant Transport in Fractured Rock*, edited by J. Bear, C. Tsang, and G. de Marsily, chap. 4, Elsevier, New York.

Clemo, T., and L. Smith (1989), Solute transport in fractured media: Dual permeability models, *Eos Trans. AGU*, *70*(43).

Clemo, T., and L. Smith (1997), A hierarchical model for solute transport in fractured media, *Water Resour. Res.*, *33*(8), 1763–1783, doi:10.1029/97WR01005.

Cvetkovic, V., J. O. Selroos, and H. Cheng (1999), Transport of reactive tracers in rock fractures, *J. Fluid Mech.*, *378*, 335–356, doi:10.1017/S0022112098003450.

Cvetkovic, V., S. Painter, N. Outters, and J. O. Selroos (2004), Stochastic simulation of radionuclide migration in discretely fractured rock near the Äspö Hard Rock Laboratory, *Water Resour. Res.*, *40*, W02404, doi:10.1029/2003WR002655.

Darcel, C., O. Bour, P. Davy, and J. R. de Dreuzy (2003a), Connectivity properties of two-dimensional fracture networks with stochastic fractal correlation, *Water Resour. Res.*, *39*(10), 1272, doi:10.1029/2002WR001628.

Darcel, C., O. Bour, and P. Davy (2003b), Stereological analysis of fractal fracture networks, *J. Geophys. Res.*, *108*(B9), 2451, doi:10.1029/2002JB002091.

de Dreuzy, J.-R., P. Davy, and O. Bour (2001), Hydraulic properties of two-dimensional random fracture networks following a power law length distribution: 2. Permeability of networks based on lognormal distribution of apertures, *Water Resour. Res.*, *37*(8), 2079–2095, doi:10.1029/2001WR900010.

Delay, F., P. Ackerer, and C. Danquigny (2005), Random walk particle tracking for solute transport in porous and fractured formations: A review, *Vadose Zone J.*, *4*, 360–379, doi:10.2136/vzj2004.0125.

Dershowitz, W. (1985), Rock joint systems, PhD. thesis, Mass. Inst. of Technol., Cambridge.

Dershowitz, W., G. Lee, J. Geier, T. Foxford, P. La Pointe, and A. Thomas (1998), FracMan—Interactive discrete fracture data analysis, geometric modeling, and exploration simulation, version 2.6, users guide, 189 pp., Golder Assoc. Inc., Denver, Colo.

Dershowitz, W., T. Eiben, S. Follin, and A. Andersson (1999), SR 97-Alternative models project, Discrete fracture network modelling for performance assessment of Aberg, *SKB Rep., R-99-43*.

Fisher, N. I., T. Lewis, and B. J. J. Embleton (1987), *Statistical Analysis of Spherical Data*, p. 329, Cambridge Univ. Press, Cambridge.

Gelhar, L. W., C. Welty, and K. R. Rehfeldt (1992), A critical review of data on field-scale dispersion in aquifers, *Water Resour. Res.*, *28*(7), 1955–1974, doi:10.1029/92WR00607.

Gräsle, W., W. Kessels, H. Kümpel, and X. Li (2006), Hydraulic observations from a 1 year fluid production test in the 4000 m deep KTB pilot borehole, *Geofluids*, *6*(1), 8–23, doi:10.1111/j.1468-8123.2006.00124.x.

Gustafson, G., and A. Fransson (2005), The use of the Pareto distribution for fracture transmissivity assessment, *Hydrogeol. J.*, *14*, 15–20, doi:10.1007/s10040-005-0440-y.

Haggerty, R., S. W. Fleming, L. C. Meigs, and S. A. McKenna (2001), Tracer tests in a fractured dolomite 2. Analysis of mass transfer in single-well injection-withdrawal tests, *Water Resour. Res.*, *37*(5), doi:10.1029/2000WR900334.

Harvey, C. F., and S. M. Gorelick (1995), Temporal moment-generating equations: Modeling transport and mass transfer in heterogeneous aquifers, *Water Resour. Res.*, *31*(8), 1895–1911, doi:10.1029/95WR01231.

Hatsuyama, Y., H. Otsu, T. Oya, and J. Okamoto (1993), A study on estimation of permeability of in situ rock masses by crack tensor theory, in *Proceedings of the 25th Symposium of Rock Mechanics*, pp. 313–317, Northwestern Univ., Evanston, Ill.

Hatton, C., I. Main, and P. Meredith (1994), Nonuniversal scaling of fracture radius and opening displacement, *Nature*, *367*, 160–162, doi:10.1038/367160a0.

Herbert, A., J. Gale, G. Lanyon, and R. Macleod (1991), Modeling for the Stripa Site characterization and validation drift inflow: Prediction of flow through fractured rock, *SKB Stripa Proj. Rep. 91-35*.

Hestir, K., and J. Long (1990), Analytical expressions for the permeability of random two-dimensional poisson fracture networks based on regular lattice percolation and equivalent media theories, *J. Geophys. Res.*, *95*(B13), 21,565–21,581.

Japan Nuclear Cycle Development Institute (1999), Final report of Kamaishi in situ experiment, *JNC Tech. Rep. TN7410 99-001*, Tokai-mura, Japan.

Japan Nuclear Cycle Development Institute (2000), H12 project to establish the scientific and technical basis for HLW disposal in Japan, project overview report, *JNC Tech. Rep. TN1410 2000-001*, Tokai-mura, Japan.

Johnson, C. D. (1999), Effects of lithology and fracture characteristics on hydraulic properties in crystalline rock—Mirror Lake research site, Grafton County, New Hampshire, edited by D. W. Morganwalp and H. T. Buxton, in *U.S. Geological Survey Toxic Substances Hydrology Program—Proceedings of the Technical Meeting, Charleston, South Carolina, March 8–12, 1999*, *U.S. Geol. Surv. Water Resour. Invest. Rep., 99-4018C*, *3*, 795–802.

Johnston, J. D., and K. W. McCaffrey (1996), Fractal geometries of vein systems and the variation of scaling relationships with mechanism, *J. Struct. Geol.*, *18*, 349–358, doi:10.1016/S0191-8141(96)80055-1.

Kosakowski, G., B. Berkowitz, and H. Scher (2000), Analysis of field observations of tracer transport in a fractured till, *J. Contam. Hydrol.*, *47*(2), 29–51.

Lawson, C., and R. Hanson (1974), *Solving Least Squares Problems*, 350 pp., Prentice-Hall, Englewood Cliffs, N. J.

Luo, J., O. A. Cirpka, M. Dentz, and J. Carrera (2008), Temporal moments for transport with mass transfer described by an arbitrary memory function in heterogeneous media, *Water Resour. Res.*, *44*, W01502, doi:10.1029/2007WR006262.

Mazurek, M., A. Jakob, and P. Bossart (2003), Solute transport in crystalline rocks at Äspö— I: Geological basis and model calibration, *J. Contam. Hydrol.*, *61*, 157–174, doi:10.1016/S0169-7722(02)00137-7.

Mettier, R., G. Kosakowski, and O. Kolditz (2006), Influence of small-scale heterogeneities on contaminant transport in fractured crystalline rock, *Ground Water*, *44*(5), 687–696, doi:10.1111/j.1745-6584.2006.00236.x.

Miller, I., G. Lee, and W. Dershowitz (1999), MAFIC: Matrix/fracture interaction code with heat and solute transport, version 1.6, user documentation, 87 pp., Golder Assoc., Redmond, Wash.

Molz, F. J., H. Rajaram, and S. Lu (2004), Stochastic fractal-based models of heterogeneity in subsurface hydrology: Origins, applications, limitations, and future research questions, *Rev. Geophys.*, *42*, RG1002, doi:10.1029/2003RG000126.

Moreno, L., and I. Neretnieks (1993), Fluid flow and solute transport in a network of channels, *J. Contam. Hydrol.*, *14*, 163–192, doi:10.1016/0169-7722(93)90023-L.

National Research Council (1996), *Rock Fractures and Fluid Flow—Contemporary Understanding and Applications*, 551 pp., Natl. Acad. Press, Washington, D. C.

Neretnieks, I. (1980), Diffusion in the rock matrix: An important factor in radionuclide retardation, *J. Geophys. Res.*, *85*, 4379–4397, doi:10.1029/JB085iB08p04379.

Niemi, A., K. Kontio, A. Kuusela-Lahtinen, and A. Poteri (2000), Hydraulic characterization and upscaling of fracture networks based on multiple-scale well test data, *Water Resour. Res.*, *36*(12), 3481–3498, doi:10.1029/2000WR900205.

Nordqvist, A. W., Y. W. Tsang, C. F. Tsang, B. Dverstorp, and J. Andersson (1992), A variable aperture fracture network model for flow and transport in fractured rocks, *Water Resour. Res.*, *28*(6), 1703–1713, doi:10.1029/92WR00216.

Olson, J. E. (2003), Sublinear scaling of fracture aperture versus length: An exception or the rule?, *J. Geophys. Res.*, *108*(B9), 2413, doi:10.1029/2001JB000419.

Olsson, O. (Ed.) (1992), Site characterization and validation, *Stripa Proj. Final Rep., 92-22*, Conterra AB, Uppsala, Sweden.

Outters, N., and D. Shuttle (2000), Sensitivity analysis of a discrete fracture network model for performance assessment of Aberg, *Rep. 00-48*, Swed. Nucl. Fuel Waste Manage. Co., Stockholm.

Paillet, F. L. (1993), Using borehole geophysics and cross-borehole flow testing to define hydraulic connection between fracture zones in bedrock aquifers, *J. Appl. Geophys.*, *30*, 261–279, doi:10.1016/0926-9851(93)90036-X.

Painter, S. (2006), Effect of single-fracture aperture variability on field-scale transport, *SKB R-06-25*, Swed. Nucl. Fuel Waste Manage. Co., Stockholm.

Painter, S., and V. Cvetkovic (2001), Stochastic analysis of early tracer arrival in a segmented fracture pathway, *Water Resour. Res.*, *37*(6), 1669–1680, doi:10.1029/2001WR900008.

Piggot, A. R. (1997), Fractal relations for the diameter and trace length of disc-shaped fractures, *J. Geophys. Res.*, *102*(B8), 18,121–18,126.

Poeter, E., G. Thyne, G. VanderBeek, and C. Guler (2003), Ground water in the Turkey Creek Basin of the Rocky Mountain Front Range in Colorado, edited by D. Boyer, P. Santi, and P. Rogers, in *Engineering Geology in Colorado: Contributions, Trends, and Case Histories*, *Spec. Publ. Ser.*, *55*, Colo. Geol. Surv., Denver.

Priest, S. D., and J. A. Hudson (1976), Discontinuity spacings in rock, *Int. J. Mech. Min. Sci. Geomech. Abstr.*, *13*, 135–148, doi:10.1016/0148-9062(76)90818-4.

Pyrak-Nolte, L., M. Cook, and P. Witherspoon (1987), Hydraulic and mechanical properties of natural fractures in low permeability rock, edited by G. Herget and S. Vongpaisal, in *Proceedings of the Sixth International Congress on Rock Mechanics, Montreal, Canada, August 1987*, pp. 225–231, A.A. Balkema, Rotterdam, Netherlands.

Renshaw, C. E., and J. C. Park (1997), Effect of mechanical interactions on the scaling of fracture radius and aperture, *Nature*, *386*, 482–484, doi:10.1038/386482a0.

Rouleau, A., and J. E. Gale (1985), Statistical characterization of the fracture system in the Strip Granite, Sweden, *Int. J. Rock Mech. Min. Sci. Geomech.*, *22*, 353–367, doi:10.1016/0148-9062(85)90001-4.

Sawada, A., Y. Ijiri, K. Sakamoto, and S. Watari (1999), Nuclide migration analysis in fracture host rock, *JNC, TN8400 99-093*.

Scholz, C. H., and P. Cowie (1990), Determination of total strain from faulting using slip measurements, *Nature*, *346*, 837–838, doi:10.1038/346837a0.

Schwartz, F. W., L. Smith, and A. S. Crowe (1983), A stochastic analysis of macroscopic dispersion in fractured media, *Water Resour. Res.*, *19*(5), 1253–1265, doi:10.1029/WR019i005p01253.

Seaton, W., and T. Burbey (2005), Influence of ancient thrust faults on the hydrogeology of the Blue Ridge Province, *Ground Water*, *43*(3), 301–313, doi:10.1111/j.1745-6584.2005.0026.x.

Shapiro, A. M. (2001), Effective matrix diffusion in kilometer-scale transport in fractured crystalline rock, *Water Resour. Res.*, *37*(3), 507–522, doi:10.1029/2000WR900301.

Shapiro, A. M., and P. A. Hsieh (1991), Research in fractured rock hydrogeology: Characterizing fluid movement and chemical transport in fracture rock at the Mirror Lake drainage basin, New Hampshire, edited by G. E. Mallard and D. A. Aronson, in *U.S. Geological Survey Toxic Substances Hydrology Program—Proceedings of the Technical Meeting, Monterey, CA, March 11–15, 1991*, *U.S. Geol. Surv. Water Resour. Invest. Rep.*, *91-4034*, 155–161.

Shapiro, A. M., and P. A. Hsieh (1994), Overview of research at the Mirror Lake site: Use of hydrologic, geophysical and geochemical methods to characterize flow and transport in fractured rock, edited by D. W. Morganwalp and D. A. Aronson, in *U.S. Geological Survey Toxic Substances Hydrology Program—Proceedings of the Technical Meeting, Colorado Springs, Colorado, September 20–24, 1993*, *U.S. Geol. Surv. Water Resour. Invest. Rep.*, *94-4015*.

Shapiro, A. M., P. A. Hsieh, W. C. Burton, and G. J. Walsh (2007), Integrated multi-scale characterization of ground-water flow and chemical transport in fractured crystalline rock at the Mirror Lake site, New Hampshire, edited by D. W. Hyndman, F. D. Day-Lewis, and K. Singha, in *Subsurface Hydrology: Data Integration for Properties and Processes*, *Geophys. Monogr. Ser.*, *171*, 201–225, AGU, Washington, D. C.

Sidle, R. C., B. Nilsson, M. Hansen, and J. Frederica (1998), Spatially varying hydraulic and solute transport characteristics of a fractured till determined by field tracer tests, Funen, Denmark, *Water Resour. Res.*, *34*(10), 2515–2527, doi:10.1029/98WR01735.

Smith, L., and F. W. Schwartz (1980), Mass transport: 1. A stochastic analysis of macroscopic dispersion, *Water Resour. Res.*, *16*(2), 303–313, doi:10.1029/WR016i002p00303.

Snow, D. T. (1968), Hydraulic character of fractured metamorphic rocks of the front range and implications to the Rocky Mountain Arsenal Well, *Q. Colo. Sch. Mines*, *63*(1), 167–199.

Tiren, S. A. (1989), Characterization of fracture zone 2, Finnsjon study site. Part 2: Geological setting and deformation history of a low angle fracture zone at Finnsjon, Sweden, *SKB TR-89-19*, Swed. Nucl. Fuel and Waste Manage. Co., Stockholm.

Tsang, Y. W., and C. F. Tsang (1989), Flow channeling in a single fracture as a two-dimensional strongly heterogeneous permeable medium, *Water Resour. Res.*, *25*(9), 2076–2080, doi:10.1029/WR025i009p02076.

Tsang, Y. W., C. F. Tsang, I. Neretnieks, and L. Moreno (1988), Flow and tracer transport in fractured media—A variable-aperture channel model and its properties, *Water Resour. Res.*, *24*(12), 2049–2060, doi:10.1029/WR024i012p02049.

Vermilye, J. M., and C. H. Scholz (1995), Relation between vein radius and aperture, *J. Struct. Geol.*, *17*, 423–434, doi:10.1016/0191-8141(94)00058-8.

Wallis, P. F., and M. S. King (1980), Discontinuity spacing in a crystalline rock, *Int. J. Rock Mech. Min. Sci. Geomech.*, *17*, 63–66, doi:10.1016/0148-9062(80)90007-8.

Walmann, T., A. Malthe Sørensen, J. Feder, T. Jøssang, and P. Meakin (1996), Scaling relations for the radius and widths of fractures, *Phys. Rev. Lett.*, *77*, 5393–5396, doi:10.1103/PhysRevLett.77.5393.

Walsh, J., and J. Watterson (1988), Analysis of the relationship between displacements and dimensions of faults, *J. Struct. Geol.*, *10*(3), 239–247, doi:10.1016/0191-8141(88)90057-0.

Watanabe, K., K. Obara, and E. Shinjo (1982), Investigation on distribution of fracture properties and anisotoropy of permeability in rock, in *Proceedings of Showa-57 Symposium*, pp. 57–60, Jpn. Soc. of Eng. Geol., Tokyo.

Wellman, T. P., and E. P. Poeter (2005), Estimating spatially variable representative elementary scales in fractured architecture using hydraulic head observations, *Water Resour. Res.*, *41*, W03001, doi:10.1029/2004WR003287.

Wellman, T. P., and E. P. Poeter (2006), Evaluating uncertainty in predicting spatially variable representative elementary scales in fractured aquifers, with application to Turkey Creek Basin, Colorado, *Water Resour. Res.*, *42*, W08410, doi:10.1029/2005WR004431.

Winberg, A. (1996), First TRUE Stage-Tracer Retention Understanding Experiments-Descriptive structural-hydraulic models on block and detailed scales of the TRUE-1 site, *SKB-ICR 96-04*, Swed. Nucl. Fuel and Waste Manage. Co., Stockholm.

M. C. Hill, Water Resources Discipline, U.S. Geological Survey, 3215 Marine Street, Boulder, CO 80303, USA. (mchill@usgs.gov)

A. M. Shapiro, Water Resources Discipline, U.S. Geological Survey, Reston, VA 20912, USA. (ashapiro@usgs.gov)

T. P. Wellman, Water Resources Discipline, U.S. Geological Survey, Lakewood, CO 80225, USA. (twellman@usgs.gov)